AD-A181 532 REGIONAL NETWORK SEISMICITY OF ASIA AND FREQUENCY-DEPENDENT Q(U) COLUMBIA UNIV NEW YORK D W SIMPSON ET AL 15 FEB 87 AFGL-TR-87-0049 1/1

UNCLASSIFIED F19628-85-K-0022 F/G 8/11 NL

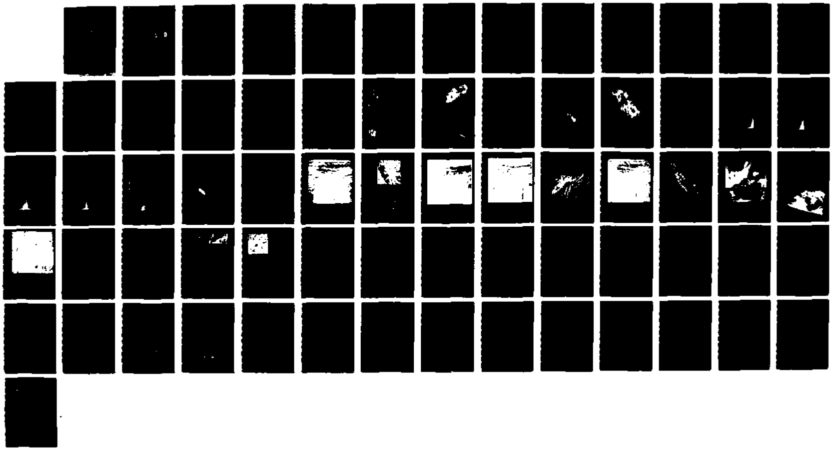

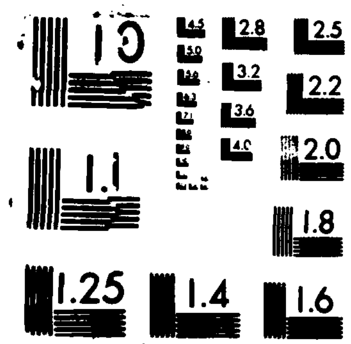
1.0
1.1
1.25
1.4
1.6
1.8
2.0
2.2
2.5
2.8
3.2
3.6
4.0
4.5
5.0

DTIC FILE COPY

(12)

AFGL-TR-87-0049

AD-A181 532

Regional Network: Seismicity of Asia: and Frequency-Dependent Q

David W. Simpson
Paul G. Richards
Arthur Lerner-Lam

Trustees of Columbia University
in the City of New York
Box 20, Low Memorial Library
New York, NY 10027

15 February 1987

Final Report
1 February 1985-30 September 1986

APPROVED FOR PUBLIC RELEASE; DISTRIBUTION UNLIMITED

AIR FORCE GEOPHYSICS LABORATORY
AIR FORCE SYSTEMS COMMAND
UNITED STATES AIR FORCE
HANSCOM AIR FORCE BASE, MASSACHUSETTS 01731

"This technical report has been reviewed and is approved for publication"

JAMES F. LEWKOWICZ
Contract Manager

HENRY A. OSSING
Branch Chief

FOR THE COMMANDER

DONALD H. ECKHARDT
Division Director

Unclassified

SECURITY CLASSIFICATION OF THIS PAGE

REPORT DOCUMENTATION PAGE

1a REPORT SECURITY CLASSIFICATION Unclassified	1b RESTRICTIVE MARKINGS
2a SECURITY CLASSIFICATION AUTHORITY	3 DISTRIBUTION/AVAILABILITY OF REPORT Approved for Public Release Distribution Unlimited
2b DECLASSIFICATION/DOWNGRADING SCHEDULE	
4. PERFORMING ORGANIZATION REPORT NUMBER(S)	5. MONITORING ORGANIZATION REPORT NUMBER(S) AFGL-TR-87-0049
6a NAME OF PERFORMING ORGANIZATION The Trustees of Columbia Univ. in the City of NY 6b. OFFICE SYMBOL (If applicable)	7a NAME OF MONITORING ORGANIZATION Air Force Geophysics Laboratory
6c ADDRESS (City, State, and ZIP Code) Box 20, Low Memorial Library New York, NY 10027	7b ADDRESS (City, State, and ZIP Code) Hanscom Air Force Base Massachusetts 01731-5000
8a. NAME OF FUNDING/SPONSORING ORGANIZATION Air Force Systems Command 8b OFFICE SYMBOL (If applicable)	9 PROCUREMENT INSTRUMENT IDENTIFICATION NUMBER F 19628-85-K-0022
8c ADDRESS (City, State, and ZIP Code) Hanscom AFB, MA 01731-5000	10. SOURCE OF FUNDING NUMBERS PROGRAM ELEMENT NO. 61101E; PROJECT NO 5A10; TASK NO. DA; WORK UNIT ACCESSION NO AH

11 TITLE (Include Security Classification)
Regional Network: Seismicity of Asia: and Frequency-Dependent Q

12 PERSONAL AUTHOR(S)
Simpson, David W.; Richards, Paul G.; Lerner-Lam, Arthur

13a. TYPE OF REPORT	13b. TIME COVERED	14. DATE OF REPORT (Year, Month, Day)	15. PAGE COUNT
Final	FROM 2/1/85 TO 9/30/86	1987 February 15	72

16 SUPPLEMENTARY NOTATION

17. COSATI CODES			18 SUBJECT TERMS (Continue on reverse if necessary and identify by block number)
FIELD	GROUP	SUB-GROUP	synthetic seismograms, regional seismicity, regional networks

19 ABSTRACT (Continue on reverse if necessary and identify by block number)

This report has three components:

1. A method is developed for the computation of body-wave synthetics which is suitable to a medium having smooth variation with depth and anelasticity having arbitrary variation with frequency. The method is applied to an anelastic earth model where Q is assumed to follow a power-law frequency dependence. The outcome is a pulse shape with properties quite different from what might be expected if the familiar constant-Q pulse shapes are surveyed.

2. The seismicity of Soviet Central Asia is studied using Soviet catalogs, and the relationship between topography and seismicity is analyzed using digital terrain data. The seismicity is concentrated along the major topographic gradients dividing the distinct physiographic/tectonic provinces of the region, with relatively low activity in both high plateaus and low basins and higher activity along the flanks of mountainous areas. Further, there is a distinct relationship between seismic activity and active ...OVER...

20 DISTRIBUTION/AVAILABILITY OF ABSTRACT ☐ UNCLASSIFIED/UNLIMITED ☐ SAME AS RPT. ☐ DTIC USERS	21 ABSTRACT SECURITY CLASSIFICATION Unclassified
22a NAME OF RESPONSIBLE INDIVIDUAL James Lewkowicz	22b TELEPHONE (Include Area Code) (617) 377-3028 — 22c. OFFICE SYMBOL AFGL/LWH

DD FORM 1473, 84 MAR

83 APR edition may be used until exhausted.
All other editions are obsolete.

SECURITY CLASSIFICATION OF THIS PAGE

Unclassified

...CONT...

salt diapirism.

3. The capabilities of the New York State Seismic Array for studying teleseismic waveforms and sub-array structure are evaluated. The array is positioned uniquely with respect to major seismogenic zones to record core phases from earthquakes with magnitudes greater than 6.0. Only minor modification of the triggering algorithm is required to lower the magnitude threshold to 5.5. Estimates of inter-station coherence are also obtained, but interpretation of the results in terms of the distribution of crustal and upper-mantle scatterers is difficult due to uncertainties in instrument response. Nevetheless, it appears as if vertically-incident signals are reasonably coherent to distances greater than 50 to 60 km, somewhat larger than observed at NORSAR and LASA in the early seventies.

CALCULATION OF BODY-WAVE PULSE SHAPES, WITH ALLOWANCE FOR FREQUENCY-DEPENDENT Q

Paul G. Richards

INTRODUCTION

The computation of body-wave synthetics, in elastic Earth models that vary purely with depth, is now routinely done by several different methods. In practice, the resulting synthetics either look the same, or differ for reasons that are quite well understood and which indicate which methods are fallible in certain situations (Helmberger and Burdick, 1979; Aki and Richards, 1980; Kennett, 1983; Richards, 1985; Chapman and Orcutt, 1985).

But, for computation of pulse shapes in anelastic models, there is a less satisfactory experience, in part because only a limited number of plausible types of attenuation have been explored to the extent of incorporation into packages for the computation of synthetic seismograms. The most common type of attenuation incorporated into synthetics is that characterized by constant Q (i.e. a Q that is frequency-independent, but which is allowed to vary with depth), which is handled by methods suggested by Carpenter (1967). But seismic data indicate that in many practical situations the assumption of a constant Q is demonstrably false. Unfortunately, once the false assumption is dropped, it is not yet clear what should replace it.

Our recent work in this area has been based on a method of computing synthetics that is effective in elastic media for situations where geometrical ray theory is accurate. These include the interpretation of body-wave waveform data for earthquakes and explosions at distances from about 30° to 85°. We first describe this method, which would hardly be needed (since there are so many other effective methods for evaluating the predictions of ray theory in elastic media that smoothly vary with depth), were it not for the generalization it allows in the case of anelastic media - generalizations that other methods usually cannot supply. Then we show an application of the method to an anelastic Earth model where Q is assumed to follow a power law frequency dependence. The outcome is a pulse shape with properties quite different from what might be expected if the familiar constant-Q pulse shapes are surveyed.

Our conclusion is, that a fundamental problem in the interpretation of body-wave broadband pulse shapes - namely, the appropriate choice of attenuation model to explain both spectral content and pulse width, and how these quantities are affected by propagation - is unresolved. But, the conventional model that uses constant Q is flawed.

RAY CALCULATIONS WITHOUT RAY TRACING

An elementary use of the relationship between travel time (T), distance (X) and intercept time (τ) concerns fitting a ray between a fixed source and receiver, and finding the geometrical spreading, without actually doing any ray tracing.

Thus, in the frequency domain, the wavefield for a generalized ray in a structure that varies solely with depth can be written

$$W(X_0, \omega) = \int f(p, \omega) \exp[i\omega\{T(p, \omega) - pX(p, \omega) + pX_0\}]\, dp \qquad (1)$$

where $T(p, \omega) - pX(p, \omega)$ is the vertical integral of vertical slowness along the ray path,

$$T - pX = \tau = \int_{\text{ray}} \sqrt{[1/v^2 - p^2]}\, dz, \qquad (2)$$

in which $v(z)$ is the velocity (complex, if there is attenuation, and also frequency-dependent if there is dispersion); and $f(p, \omega)$ includes the radiation pattern as well as relevant reflection/transmission coefficients for the generalized ray of interest. There are minor differences of detail between plane stratified and spherically stratified media. Richards (1973) obtained examples of (1) even for rays that have turning points, rather than reflection from a specific interface.

In order to obtain the ray-theory approximation for an array of receivers, consider the following six steps:

(i) One fixes ω and computes f and $\tau(p)$ for a set of equally spaced real p-values, in a range of the real ray-parameter axis that is close to where one expects complex saddle points to lie for the range of distances (i.e. X_0 - values) at which one wishes to know W. Let the increment in p here be Δp.

(ii) At fixed X_0, one searches through the array of $\mathrm{Real}[T - pX + pX_0]$ to see at which of the sampled points in p it has a minimum (or, a maximum for certain kinds of ray). Label this discrete point as p_{js}. The complex

saddle must presumably lie near this point of the real p-axis. If there is no attenuation, the saddle will lie on the real p-axis if there is a real ray between source and receiver.

(iii) Find the values (complex, if there is attenuation) of the three constants T_0, p_0, and $DXDP$ that best fit the sampled phase factor according to

$$T - pX + pX_0 = T_0 - (p - p_0)^2 \times DXDP / 2 \qquad (3)$$

in the vicinity of p_{js}. Note that if one just uses p_{js} itself, and the points just before and just after it, closed form expressions that in practice are often very accurate can easily be given for p_0, T_0, and $DXDP$. Aki and Richards (1980) introduce the function $J(p) = T - pX + pX_0$ (see their page 423). In terms of this sampled function,

$$J_{js-1} = J(p_{js-1}) = T_0 - (p_{js} - p_0)^2 \times DXDP / 2 + \Delta p \, . \, p_0 \, . \, DXDP - (\Delta p)^2 . \, DXDP / 2$$

$$J_{js} = J(p_{js}) = T_0 - (p_{js} - p_0)^2 \times DXDP / 2$$

$$J_{js+1} = J(p_{js+1}) = T_0 - (p_{js} - p_0)^2 \times DXDP / 2 - \Delta p \, . \, p_0 \, . \, DXDP - (\Delta p)^2 . \, DXDP / 2.$$

Therefore, the closed form expressions for the desired constants are

$$DXDP = - [J_{js+1} - 2 J_{js} + J_{js-1}] / (\Delta p)^2 ,$$

$$p_0 = - [J_{js+1} - J_{js-1}] / (2. \Delta p \, . \, DXDP)$$

and finally

$$T_0 = J_{js} + (p_{js} - p_0)^2 \times DXDP / 2. \qquad (4)$$

The point of this exercise, of course, is that p_0 is an estimate of the position of the complex saddle; T_0 is an estimate of the complex travel time; and $DXDP$ (signifying dX/dp at the saddle) is the relevant constant, complex in general, needed to evaluate geometrical spreading.

(iv) Interpolate from $f(p_{js}, \omega)$ and $f(p_{js+1}, \omega)$ to evaluate $f(p_0, \omega)$.

(v) Claim that the saddle point approximation to W is

$$W(X_0, \omega) = f(p_0, \omega) \exp(i\omega T_0) \times \sqrt{[2\pi \div (i\omega . DXDP)]}. \qquad (5)$$

Choose the next value of X_0, and loop back to the second step to do various distances. Choose the next value of frequency ω, and loop back to the first step. This loop is necessary only if Q is frequency-dependent, and/or if there is allowance for body-wave dispersion. Also, for some types of anelasticity, it may be possible to abbreviate this step and estimate more directly the global frequency-dependence of the saddle-point approximation.

(vi) Finally, one can go to the time domain:

$$W(X_0, t) = (1/2\pi) \int W(X_0, \omega) \exp[-i\omega t] \, d\omega. \tag{6}$$

Note that the whole effort is accomplished using real values of ray-parameter, at the time-consuming stage of tabulating f and τ at discrete p values. Often, the dependence on frequency in (5) is sufficiently simple that (6) can be evaluated explicitly.

The method allows easily for investigation of different attenuation-dispersion pairs. This is handled just by insertion of some appropriate rule for evaluating $v(z, \omega)$, and then recognizing that $\tau = \tau(p, \omega)$. For example, in a constant Q medium in which the method of Carpenter (1967) is used to handle dispersion, the real body-wave velocity $v_e(z)$ of an elastic model is replaced by

$$v(z, \omega) = v_e(z) \{ 1 + [1 / Q(\omega)] [(1 / \pi) \ln (\omega / \omega_0) - i / 2] \} \tag{7}$$

The method is simple and rapid to execute, and has been found quite accurate for 1-D (that is, purely depth-dependent) problems (Richards, 1985). A comparison of synthetics produced by this method and Cagniard first motion method is given here in Figure 1.

A series of papers by Borcherdt (most recently, Borcherdt *et al.*, 1986) has drawn attention to the need for more careful handling of attenuation. Specifically he has advocated working with plane waves that may propagate in a direction that differs from the direction of most rapid attenuation. (The "direction of propagation" is the direction of most rapid phase increase.) He has shown that such waves have properties that much conventional analysis (i.e., that based on plane waves propagating in the direction of maximum attenuation) cannot reproduce. Fortunately, the method based on (1) through (5), which finds stationary values of the ingrand at complex values of horizontal slowness, gets around Borcherdt's

valid objections to conventional analysis, yet does so for attenuating media in a way that requires little change from computational experience with elastic media. The subject is further discussed in Richards (1984). Incidentally, we note here that the whole procedure has recently been generalized so that it carries over to 3-D problems in layered structures, with planar interfaces that can have any strike and dip. In effect one can develop a generalized ray theory for a medium built up from a stack of arbitrary wedges, and the geometrical ray approximation can be computed by a method that is an extension of (1) to (7) (Richards - 1987 proposal to the National Science Foundation).

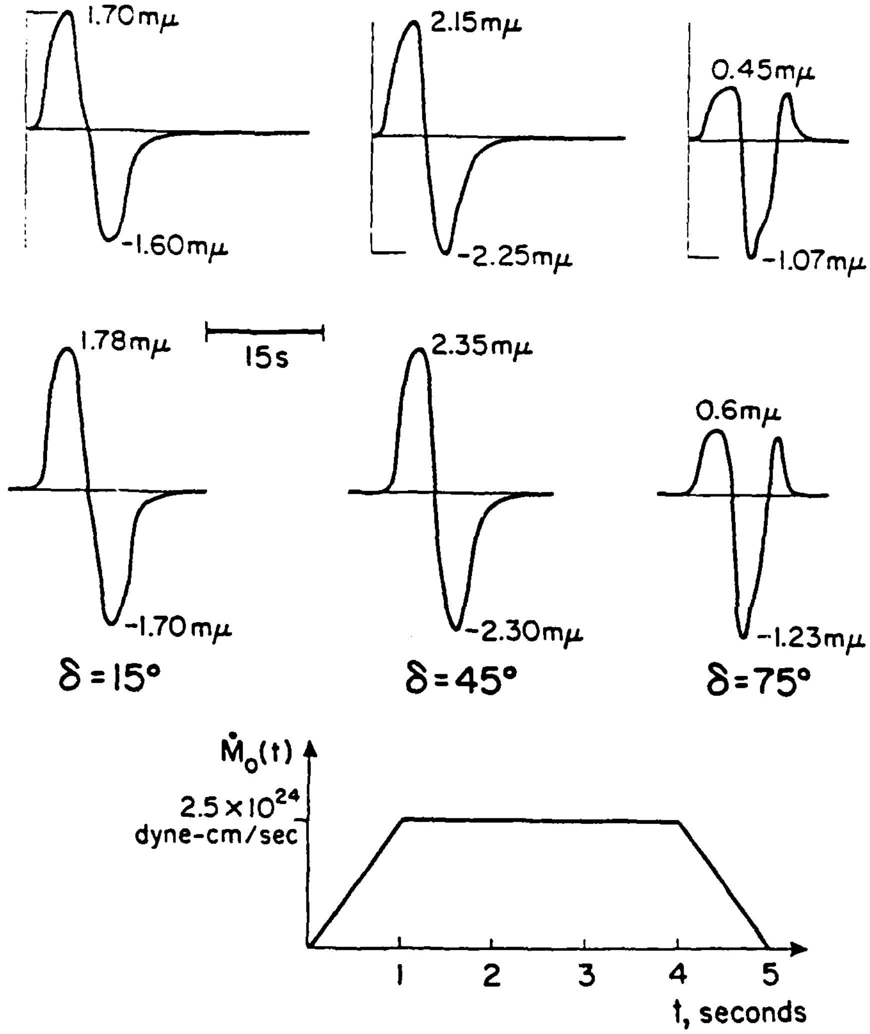

Fig. 1. Each pulse gives the P-wave group ($P+pP+sp$) at distance 80°, and 30° off the strike direction, from a point source 15 km deep. Rake is 90°, and results are given for three different dips. These are displacements in the upward vertical direction (after a free surface correction). t^* is taken as 1 second, and the time dependence of the source is given at the bottom of the figure.

The upper row uses a Cagniard first motion approximation [Langston and Helmberger, 1975]. The lower row (which has the same time scale but is displayed with a slightly different amplitude scale) uses the complex saddle point spectral method reviewed in the text, with model PEM-C and a Q structure that gives $t^* = 1$ at 80°.

Numbers displayed are displacement in $m\mu$. The two methods, each of which is basically geometrical ray theory adapted to an attenuating medium, agree to within about 10%.

EXAMINATION OF BODY-WAVE PULSE SHAPES IN DIFFERENT TYPES OF MEDIA

We have used the method based on (1) through (7) to compare pulse shapes in three different Earth models. We have used a fixed source-receiver distance, one for which geometrical ray theory is usually deemed adequate even for broad-band body wave pulses, so that attention can be focussed on the single issue of what effects result from different choices about the frequency-dependence of Q.

Thus, in Figure 2 is shown the P-wave pulse shape from an impulsive source in Earth model SL8, for which Q is constant and quite low in value. Note the charateristic features of this pulse: high frequencies have been selectively removed, and the pulse shape is broadened with an asymmetric rise and fall. The attenuation-dispersion pair is based on equation (7).

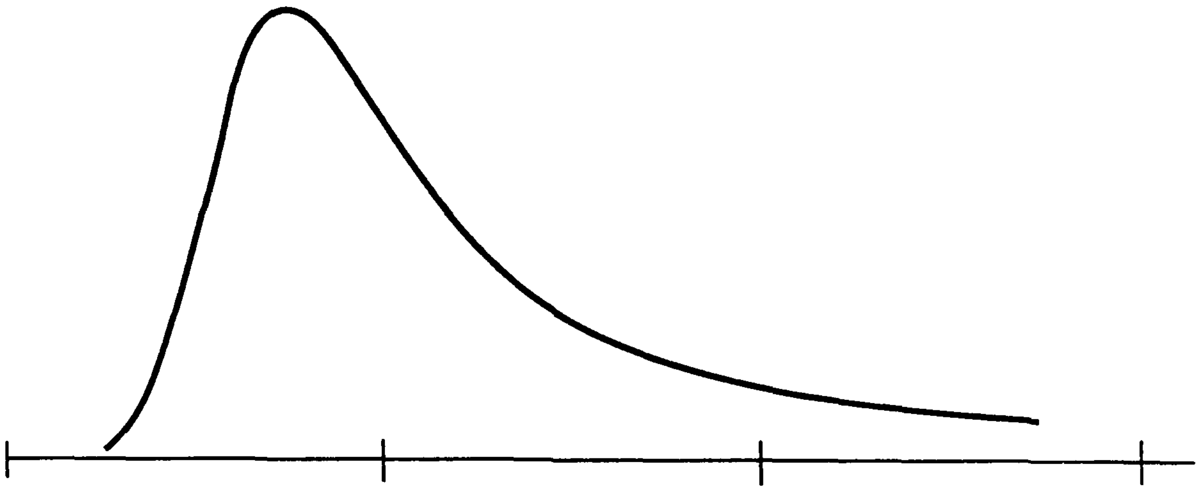

Figure 2. The P-wave pulse at 48° in Earth model SL8, for an impulsive shallow source. Constant Q, Carpenter law. Tick marks are at 1 s intervals.

In Figure 3 is shown the same pulse, but for Earth model AFL (i.e. from Archambeau, Flinn and Lambert, 1966). Q is again constant, but is significantly higher than the value for SL8.

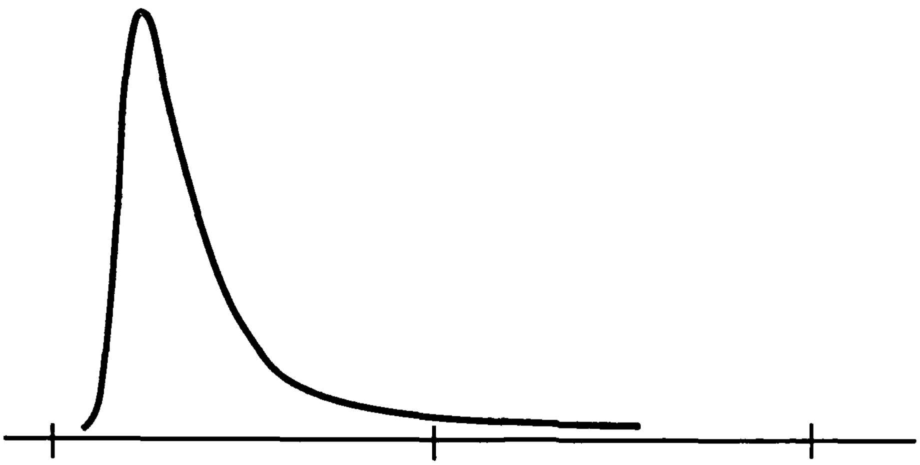

Figure 3. The P-wave pulse shape at 48° in Earth model AFL, from a shallow impulsive source. Tick marks, 1s.

Since both AFL and SL8 are data-driven anelastic Earth models, the first based on relatively high frequency signals (about 2 Hz) and the second based on relatively low frequencies (about 0.005 Hz), it is clearly unsatisfactory that each model is presented in terms of a frequency-independent Q structure. That is, Q is constant and has low value in SL8; Q is constant but with a high value in AFL. Various high-frequency phenomena displayed in seismic data are not present in SL8, and low frequency phenomena in seismic data are not present in AFL.

It is therefore appropriate to consider some kind of interpolation for Q across the frequency range whose extremes are represented by the frequency values typical of the data bases underlying these two Earth models. We have done this by assuming a Q that has a power-law dependence on frequency,

$$Q(\omega) = Q_0 \, (\omega / \omega_0)^{1-s} \tag{8}$$

for some choice of constant s. Q_0 is a constant, the value of $Q(\omega)$ at frequency ω_0.

We find from causality rules and the evaluation of Hilbert transforms

that the appropriate replacement for equation (7) is now

$$v(z, \omega) = v_e(z) \{ 1 + [1 / 2 Q (\omega)] [((Q(\omega) / Q_0) - 1) \tan (s\pi/2) - i] \}. \qquad (9)$$

Consideration of the difference in frequency ranges over which SL8 and AFL were generated, and the values of the two separate but constant Q values in each model, leads one to a value of about 0.7 for the constant s that appears in equation (8). Thus, Q has about a 0.3 power-law dependence on frequency, to fit the two kinds of data base underlying these models.

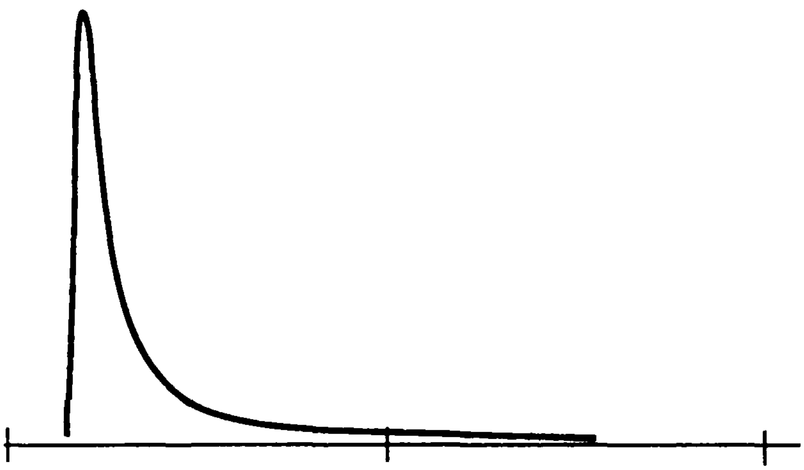

Figure 4. The P-wave at 48° in an Earth model with power-law Q, having approximately the Q of SL8 at frequencies for which the attenuation in SL8 was determined, and the Q of AFL at frequencies for which the attenuation of AFL was determined. Impulsive shallow source. Tick marks, at 1s intervals.

The outcome of computing a pulse shape based on this $Q(\omega)$ might reasonably be expected to be a pulse somewhat intermediate between those of Figures 2 and 3, since we have merely found a way to interpolate for Q across a broad band of frequencies that is representative of SL8 at one end, and AFL at the other. But the actual outcome is different. It is shown in Figure 4, and one sees a pulse shape that has an even shorter rise time than does that of Figure 3 for AFL. The reason turns out not to be hard to find. It is, that at frequencies even higher than those which charaterize the data base for AFL, equation (8) gives a higher value of Q than the constant Q value of AFL itself. Since it is the highest frequencies

that determine the rise time, this latter feature will, in the frequency-dependent Q model, be reflective of the assumptions built into (8) concerning the very-high frequency dependence of Q. In this case, Q is unbounded as frequency rises, which presumably is why the rise time is so short in Figure 4.

We therefore reach two conclusions. First, that a constant Q attenuation model is unsatisfactory . (This has long been known: such a model does not explain observations across the observed range of frequencies.) Second, that its replacement is not obvious. Artificial features, associated with attenuation laws applied outside the range of frequencies for which there is a good data base, can in the time domain be drawn into the appearance of a pulse shape computed within the frequency band at which data is acquired. Another example of this general problem was given by Richards (1985) in connection with an attenuation law appropriate for a spectrum of relaxation mechanisms.

A good research plan to resolve this issue is to see if high-quality broad-band pulse shape data can be acquired, for example from RSTN body-wave data of deep earthquakes observed teleseismically. It may then be possible to obtain the attenuation-dispersion pair directly from the data. We note a first attempt in this direction (Choy and Cormier, 1986). It is difficult to achieve results, because of the need to remove source effects, and effects of heterogeneity of structure at depth (e.g. the downgoing slab, which is always present as a cause of the earthquake activity itself). However, we are confident that an observational program will indeed result in suggestions for the attenuation-dispersion pair that is appropriate in computation of synthetics, and that will narrow the range of current trade-offs between source and propagation phenomena.

References.

Aki, K., and P.G. Richards, *Quantitative Seismology - Theory and Methods, vol. I*, W.H. Freeman and Co., San Francisco, 1980.

Archambeau, C.B., E.A. Flinn, and D.G. Lambert, Fine structure of the upper mantle, *J. Geophys. Res., 74*, 5825-5866, 1966.

Borcherdt, R.D., G. Glassmoyer, and L. Wennerberg, Influence of welded boundaries in anelastic media on energy flow, and characteristics of *P*, *S*-I, and *S*-II waves: observational

evidence for inhomogeneous body waves in low-loss solids, *J. Geophys. Res., 91*, 11503-11518, 1986.

Carpenter, E.W., Teleseismic signals calculated for underground, underwater, and atmospheric explosions, *Geophysics, 32*, 17-32, 1967.

Chapman, C.H., and J.A. Orcutt, The computation of body wave synthetic seismograms in laterally homogeneous media, *Rev. Geophys., 23*, 105-163, 1985.

Choy, G.L., and V.F. Cormier, Direct measurement of the Mantle attenuation operator for Broadband *P* and *S* waveforms, *J. Geophys. Res., 91*, 7326-7342, 1986.

Helmberger, D.V., and L.J. Burdick, Synthetic seismograms, *Ann. Rev. Earth Planet. Sci., 34*, 417-442, 1979.

Kennett, B.L.N., *Seismic Wave Propagation in Stratified Media*, Cambridge University Press, 1983.

Langston, C.A., and D.V. Helmberger, A procedure for modeling shallow dislocation sources, *Geoph. J. Roy. astr. Soc., 42*, 117-130, 1975.

Richards, P.G., Calculation of body waves, for caustics and tunnelling in core phases, *Geoph. J. Roy. astr. Soc., 35*, 243-264, 1973.

Richards, P.G., On wavefronts and interfaces in anelastic media, *Bulletin of the Seismological Society of America, 74*, 2157-2165, 1984.

Richards, P.G., *Seismic wave propagation effects -- development of theory and numerical modelling*, Chapter in DARPA commemorative volume "The VELA Program: A Twenty-Five Year Review of Basic Research", ed. A.U. Kerr, pp. 183-251, 1985.

SEISMICITY OF CENTRAL ASIA

D.W. Simpson

Soviet Earthquake Catalogs

The Institute of Physics of the Earth, Moscow issues an annual catalog of earthquakes in the USSR (Zemletriaseniia v SSSR, hereafter ZSSSR). These annual volumes contain articles and catalogs for different subregions of the USSR, based on seismic regionalization. The largest of these catalogs is for Central Asia, the active region along the USSR's southern border.

The Central Asia region includes the territory of the republics of Tadjikistan, Kazkakhstan, Uzbekistan, Kirghizia and Turkmenia (Figure 1). The main physiographic divisions included are the Northern and Southern Tien Shan and Pamir Mountains, Tadjik Depression, Kyzul Kum desert and Hindu Kush (Figure 2b). The area covered by the ZSSSR catalog extends beyond the borders of the USSR into Iran, Afghanistan and China to the south. Coverage of these border regions becomes less complete, however, because of the lack of stations in southern azimuths.

Comparison of ISC and ZSSSR catalogs

The increased coverage with regional and local stations results in a Soviet catalog that has a lower detection threshold and higher resolution than that of teleseismic catalogs such as the International Seismological Center (ISC). Figure 3 shows the annual and cumulative numbers of earthquakes reported by ISC and ZSSSR for the period 1964 - 1979 and maps derived from the two catalogs are shown in Figures 4 and 5.

The availability of a detailed catalog for Central Asia, compiled entirely from local data sources provides an interesting opportunity to examine the completeness and accuracy of the ISC catalog. Unfortunately, the ZSSSR and ISC catalogs are not completely independent, since some of the Soviet data are provided to and used by ISC. Only a subset of stations are reported to ISC however, so that the ZSSSR catalog can be assumed to be more accurate and, because of the increased density of stations, it is certainly more complete.

We have used an algorithm based on nearness in space and time to identify entries for common events in the two catalogs. Of the 3720 events reported by ISC for 1964-1978, 3602 are found in ZSSSR. Most of the events reported by ISC but not found in ZSSSR are either of low magnitude and located near the southern limits of the Soviet catalog or are poorly determined locations (i.e. reported by less than 5 stations). The only well located events above magnitude 5.0 reported only by ISC within the area well covered by ZSSSR are events identified as peaceful nuclear explosions.

For those events that are common to both catalogs, we have determined the differences in location parameters (dx - longitude, dy - latitude, dr - epicenter ($=\sqrt{(dx^2+dy^2)}$), dz - depth, dt - origin time and dm - magnitude).

Epicentral location - Map views of the differences in location(dx, dy), as a function of number of stations used by ISC, are shown in Figure 6. The origin is the ZSSSR location for each event with points placed at the end of the vector connecting the ZSSSR and ISC locations. The difference in epicentral location (dr) is shown in Figure 7. For locations determined with less than 10 stations, differences of over 200 km are observed. The difference in location decreases as the number of stations used by ISC increases (usually a direct function of the magnitude). The differences in location are smaller in the EW direction and there is an absolute bias to the north, both most likely resulting from the paucity of ISC reports from stations to the north. For events for which more than 50 stations

are available in the ISC solution, the standard deviation in the difference between the ISC and ZSSSR location drops to about ±12 km, with the ISC locations biased about 10 km to the ESE of those given by ZSSSR.

Depth and origin time - Figures 8 and 9 show the differences in depth (dz) and origin time (dt) as a function of the number of stations used in the ISC location. While dr (Figure 7) shows the gradual decrease with number of stations, both dz and dt show broad and biased (>0) distributions even beyond 100 stations.The bias towards late origin times and greater depths apparent in Figures 8 and 9 results from the well-known trade-off between these two parameters in the earthquake location process. Many of the catalogs entries report no depths or standard depths of 0 km (ZSSSR) or 33 km (ISC). Figures 10 and 11 remove these "unknown" depths and attempt to classify the remaining data in terms of events which we can be confident are actually deep or shallow and those in which one of the catalogs is in error. In Figure 10 we assume that those events for which both ISC and ZSSSR report depths greater than 60 km are actually deep. In this case the distribution of dt is symmetrical about zero. We assume that events that are assigned shallow depths by both catalogs (but not 0 km in ZSSSR or 33 in ISC) are actually shallow. Figures 11 and 12 show that for these shallow events there is a clear tendency for the ISC origin times to be later (average of 3 s), which is compensated for (Figure 12) by the ISC depths being deeper.

Magnitude - The Soviet classification of earthquake size is energy class, k, where k is the log of energy release in joules. Rautian (1960) gives the following relationship , based on an analysis of determinations of both magnitude and energy class for regional and local earthquakes:

$$m = (k-4)/1.8$$

or

$$k = 1.8m + 4$$

Figure 13 shows the relationship between k as reported in the ZSSSR catalog and m_b for those events with magnitude reported by ISC. The relationship found:

$$k = 1.93m + 3.29$$

is similar to that reported by Rautian.

SEISMICITY AND TOPOGRAPHY

Many of the topographic features of Central Asia can be discerned in the patterns of seismicity from the Soviet Catalog in Figure 2 and 5. Among the more prominent features:

a) There is intense activity along the southern front of the northern and southern Tien Shan. This zone, the Gissar Kokshal seismic zone, is the site of the largest earthquakes in Central Asia (Leith and Simpson, 1986a) and marks the southern edge of what can be clearly identified as part of the "original" Asian plate.

b) Realtively low levels of seismicity are found within the high mountainous areas. The Gissar and Kokshal Ranges of the Tien Shan are flanked on the south and north by high seismicity, but the higher elevations are much less active. Relatively low levels of activity in regions of high elevaiton are also found in the Talas Fergana Ranges and the highest section of the Pamir.

c) Relatively low levels of seismicity are found within the major intermountain basins and depressions. Most prominent of these is the Issyk Kul Basin, where high activity along the ranges bordering the basin clearly outlines the relatively low seismicity of the basin itself. The Fergana Valley is similar but less obvious. The Tadjk Depression and Tarim Basin have high activity on their northern edges, near the Gissar Kokshal zone, but are less active in their interiors.

The seismicity is thus concentrated along the major topographic gradients dividing the distinct physiographic/tectonic provinces of the region, with relatively low activity in both high plateaus and low basins and higher activity along the flanks of the mountainous areas.

Digital Terrain Data

To study the relationship between topography and seismicity in more detail, we have obtained digital terrain data for Central Asia from the Defense Mapping Agency (DMA) topographic database. Topographic elevations are provided at 3" intervals (1200 points per degree or approximately 100 m spacing).

We have carried out preliminary analysis of segments of these data making extensive use of the International Imaging Systems (I^2S) image processor at Lamont Doherty. The original data are provided in blocks of 1° x 1° (1200 x 1200 points). While that resolution has been useful in some detailed studies (e.g. the Kulyab salt dome study described below or as part of our work on induced seismicity at Nurek reservoir), the volume of data is too large for synoptic studies of large areas and it is necessary to severely decimate the data. The image processing system provides a convenient environment for reading the data, creating and examining full resolution images, decimating into smaller panels and creating mosaics of larger map areas. The image processor can also be used to apply different enhancement techniques to the topographic images, combine the topography with other (eg. epicenter) data and show the results in glowing color. In this report we limit ourselves to low resolution greyscale versions of these images.

Tadjik Depression and Southern Tien Shan

An example of an image created from the terrain data is shown in Figure 14. This area includes the Southern Tien Shan (Gissar and Zeravshan Ranges), Tadjik Depression and western Pamir. This is the most active part of Soviet Central Asia and has been extensively studied by Soviet groups at the Tadjik Institute of Seismoresistant Construction and Seismology (TISSS) in Dushanbe and the Complex Seismological Expedition (KSE) in Garm, an outpost of the Insititute of the Physics of the Earth, Moscow. It is also the site of our earlier work on induced seismicity at Nurek Reservoir (*Simpson and Negmatullaev 81, Keith et al 82, Leith et al 81*) and regional tectonics (Kristy and Simpson 1980, Leith and Alvarez 1985, Leith and Simpson 1986a,b). Figure 15 identifies in more detail some of the geographic features in a subsection of Figure 14 near Nurek reservoir.

Figure 16 represents topography with intensity directly proportional to elevation. In Figure 17 a filter has been used to locally enhance the contrast within different topographic provinces. Thus the relationship between intensity and elevation is no longer linear or spatialy constant, but many of the subtle topographic features are more clearly distinguished. In Figure 18 a simple shaded relief map has been produced by taking the first spatial derivative of the elevation in the NW-SE direction, giving the impression of illumination from the NW. This filter accentuates NE-SW striking features (eg. ridges in the Tadjik Depression). A similar image, with illumination from the NE (Figure 19) accentuates features perpendicular to those in Figure 18.

One of the first order features obvious in Figures 16-19 is the contrast between the topographic style in the northern half of the image and that in the south. The northern segment, with higher and smoother average topography, a general EW fabric and deeply incised rivers is composed primarily of Paleozoic granites of the Southern Tien Shan. The southern part, with pronounced, sharp ridges oriented more NE-SW, shows the results of recent folding and thrusting of the young foreland fold and thrust belt of the Tadjik Depression (Leith and Alvarez, 1985). The seismicity of this area (Figure 20) and its relationship to the major physiographic provinces is described in detail by Leith and Simpson (1986a). Three clear types of seismicity are found in the shallow earthquakes of the region (in addition to the intermediate depth activity of the Hindu Kush). The infrequent, large earthquakes (up to $M=8^+$) are confined to the Gissar Kokshal zone, along the front of the Southern Tien Shan, but that zone has a relatively low level of microearthquake activity. The greatest concentration of seismicity, in terms of numbers, is within the sediments of the Tadjik Depression, but there are few events here with magnitude greater than 5.5. Beneath the sediments, the third type of seismicity is that within the basement itself. The activity in the Depression is especially high in its northeastern end near

Garm, in the area of greatest convergence between the Pamir and Tien Shan. In this area, the sediments have been thrust up and out of the Depression itself, onto the Gissar Kokshal zone, producing a complex three dimensional distribution of seismicity in which all three types of activity overlap (Leith and Simpson, 1986a).

Salt Domes and Seismicity near Kulyab, Tadjikistan

A strong concentration of shallow seismicity (up to magnitude 5) stands out in the relatively low activity of the southern Tadjik Depression near the town of Kulyab (Figure 20). There are also large salt domes exposed at the surface in this same region. We have used Landsat and topographic data in conjunction with the seismicity catalog to investigate the correlation between the seismicity and the salt domes (Leith and Simpson, 1986b).

Figure 21 shows a black and white version of the Landsat image for the Kulyab area. Areas of high infrared return (vegetation) have been set black in this image so that the dark regions in valleys are irrigated farm land. The two light colored circular features are salt domes. Figure 22 shows a perspective view (from the SW) derived by creating a 3D image from the digital terrain data and adding texture from the Landsat image. The major dome to the south (Mumin dome) is devoid of vegetation and stands 870 meters above the surrounding plain. The high topography beyond the Mumin dome is associated with the Sari-Chashma salt diapir, a buried structure identified in geophysical surveys. Figure 23 shows the original and shaded relief versions of the topographic data with seismicity superimposed. Most of the cluster of seismicity in the southeastern corner of the image followed a m=5.2 earthquake on April 2, 1973.

It is our conclusion (Leith and Simpson, 1986b) that the seismicity is clearly related to the salt doming. The highest level of current activity is not located at one of the domes which has pierced the surface, but is near the buried Sari-Chashma diapir, a buried structure which appears to be actively rising. Because of the lack of depth control in the Soviet hypocentral locations, it is not clear whether the earthquakes result from increased stress within the sediments above the dome structure or are related to fracturing near or within the salt layer at depth. To our knowledge, this is the only reported case of seismicity associated with active salt doming. More detail is to be found in Leith and Simspon (1986b, included as appendix to this report).

Figure 1 Soviet Central Asia and surrounding areas.

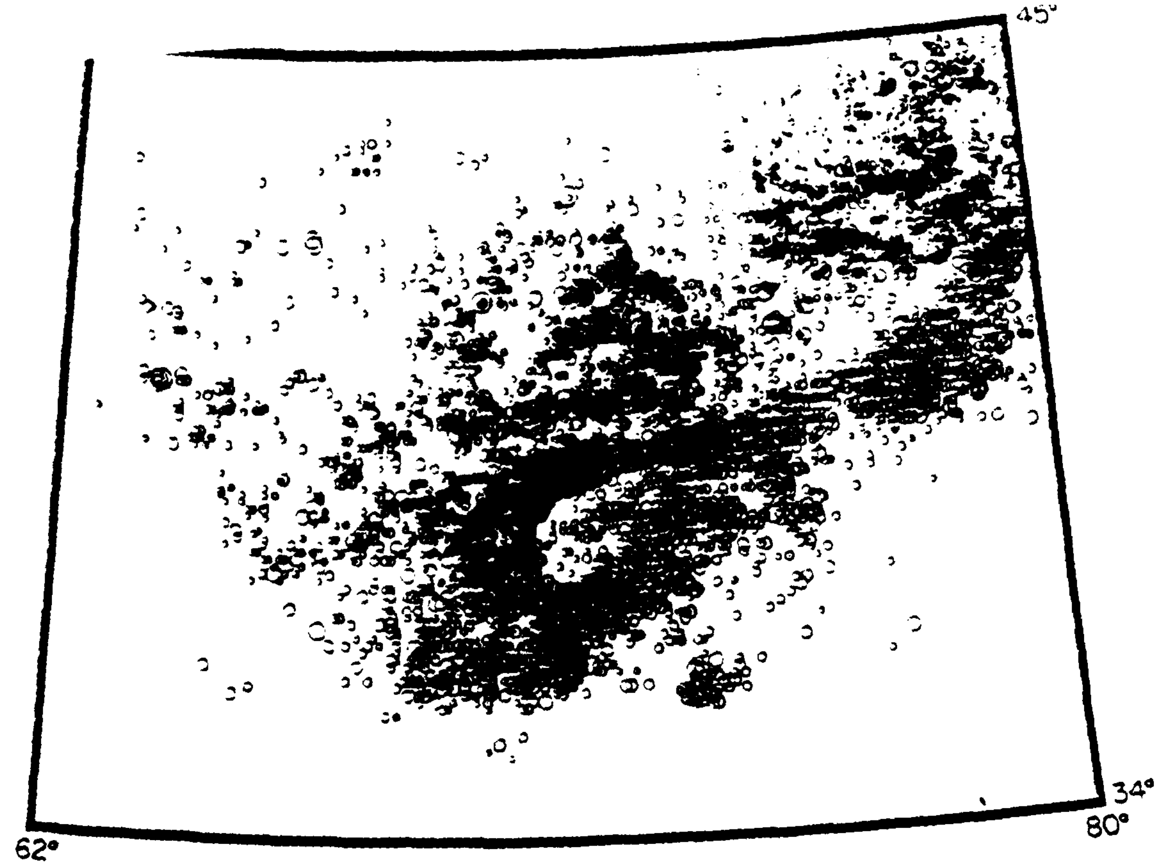

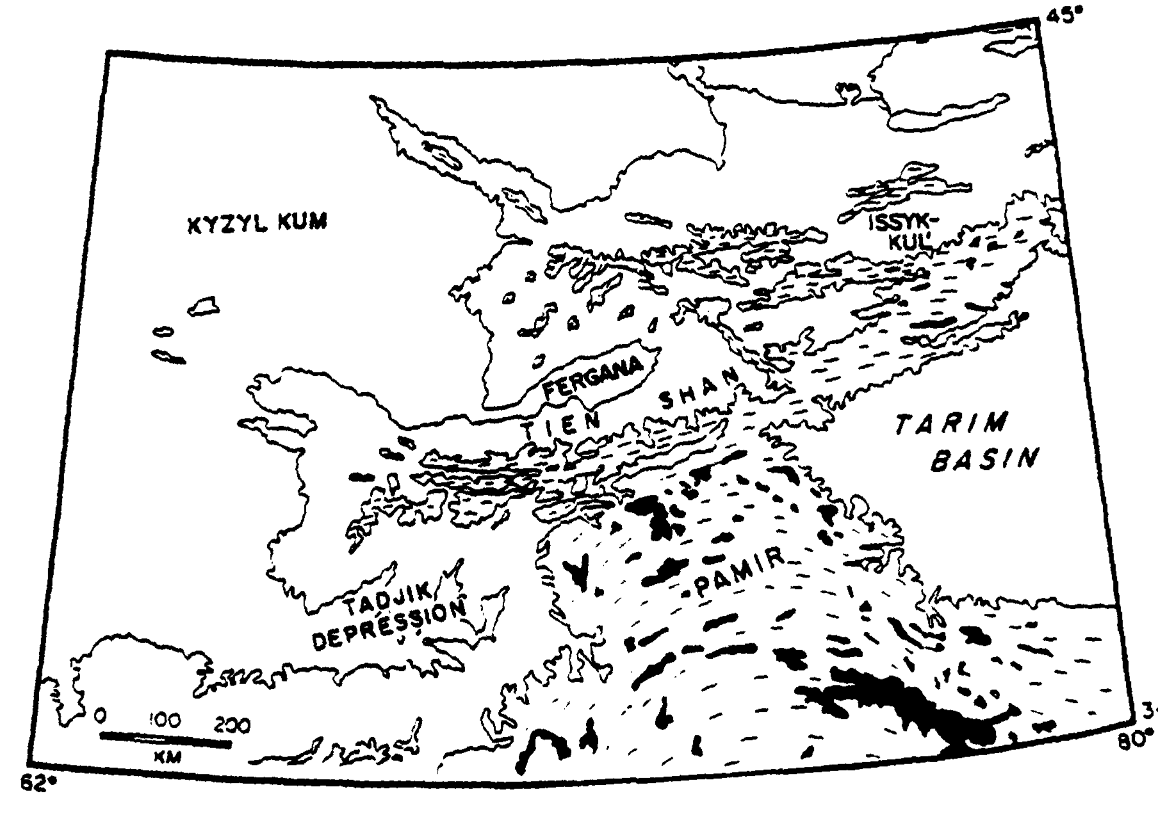

Figure 2 Epicenter map of earthquakes in ZSSSR 1964-1977. A comparison with the simplified topographic map (bottom, same area) shows that many of the active seismic zones occur along the edges of the major mountain ranges, with relatively low activity within the the ranges themselves and within major basins.

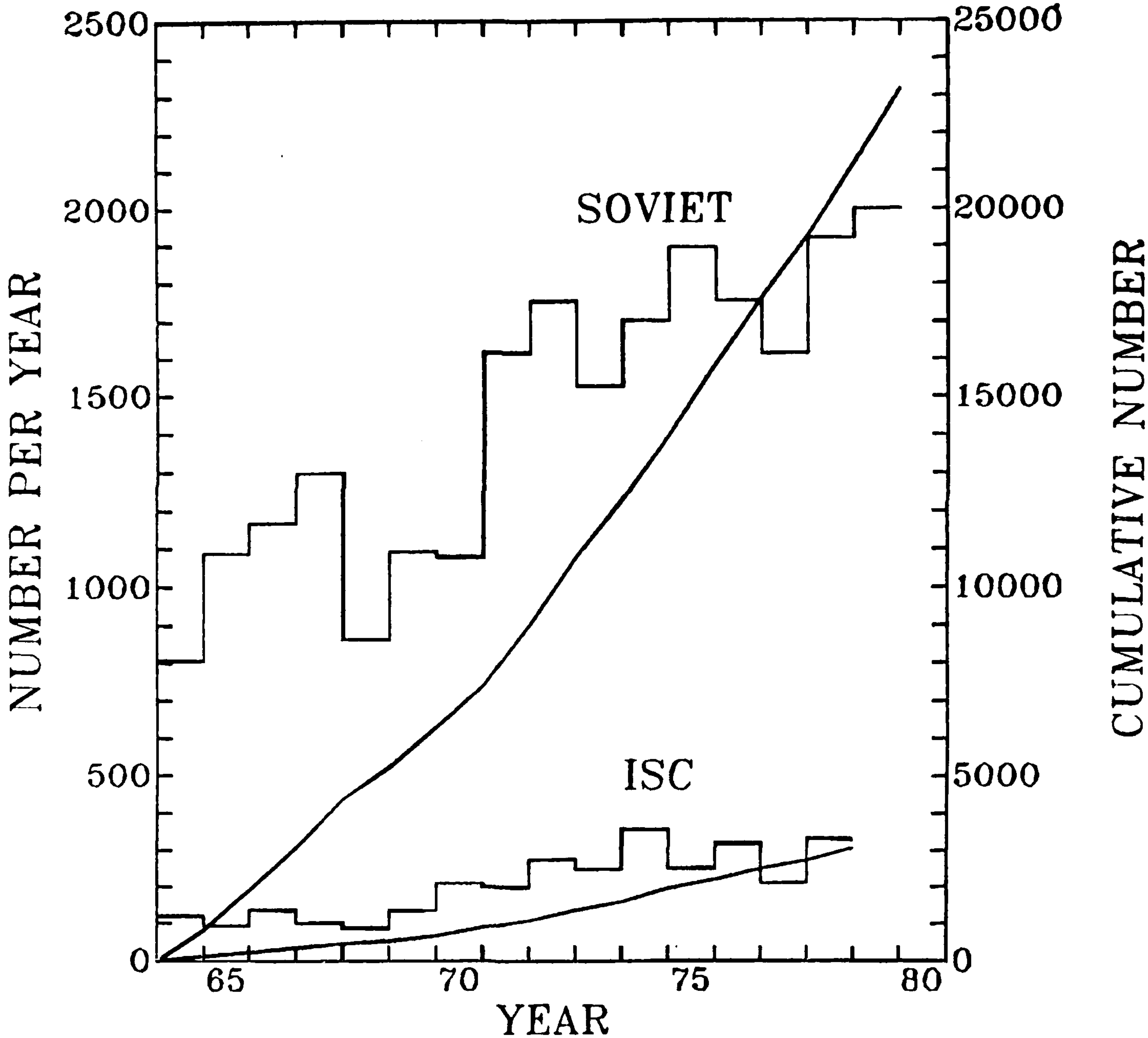

Figure 3 Cumulative and annual numbers of earthquakes in the ZSSSR and ISC catalogs.

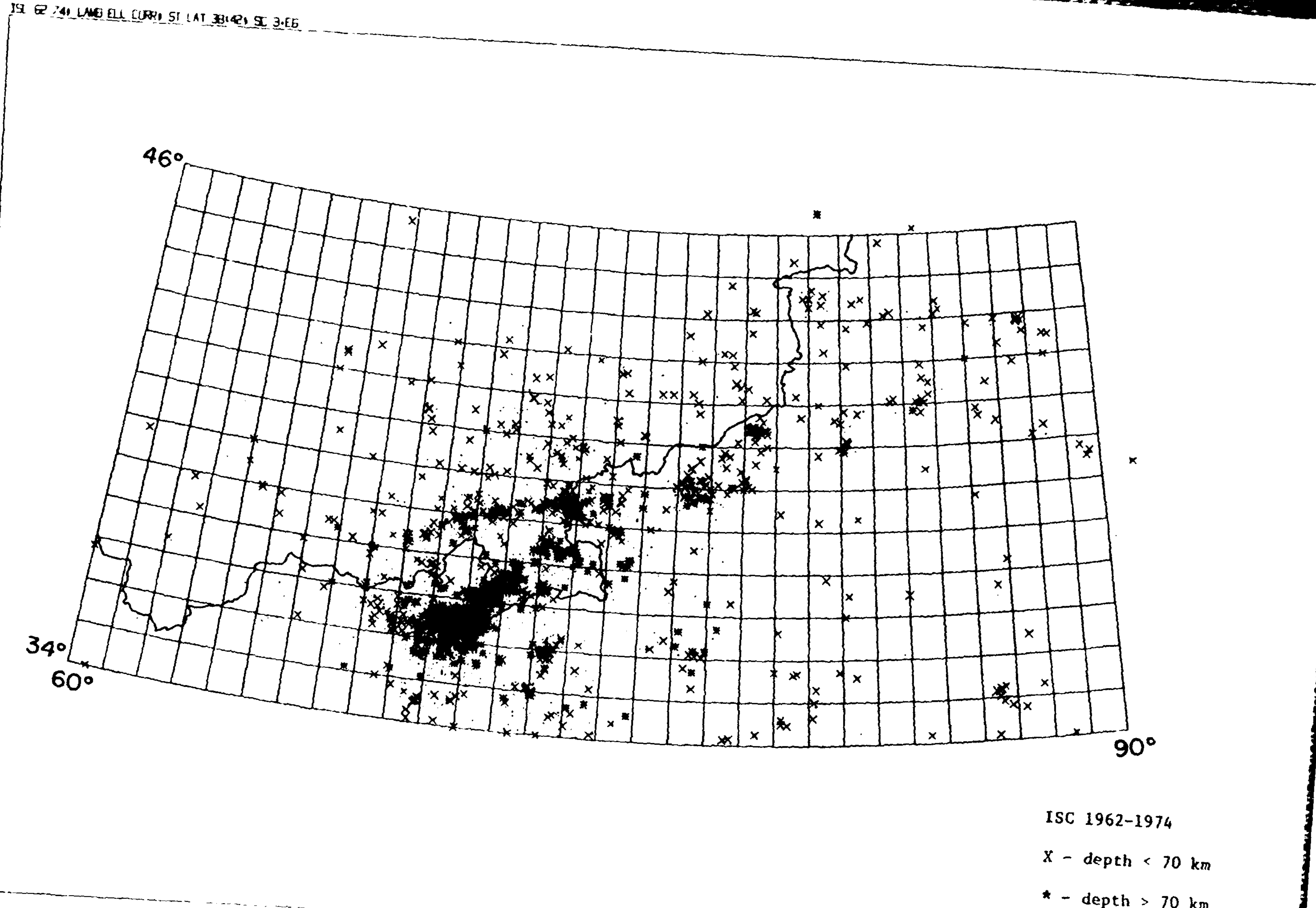

Figure 4 Epicenter map of earthquakes in ISC catalog 1962- 1974.

Figure 5 Epicenter map of earthquakes in ZSSSR catalog 1964-1977.

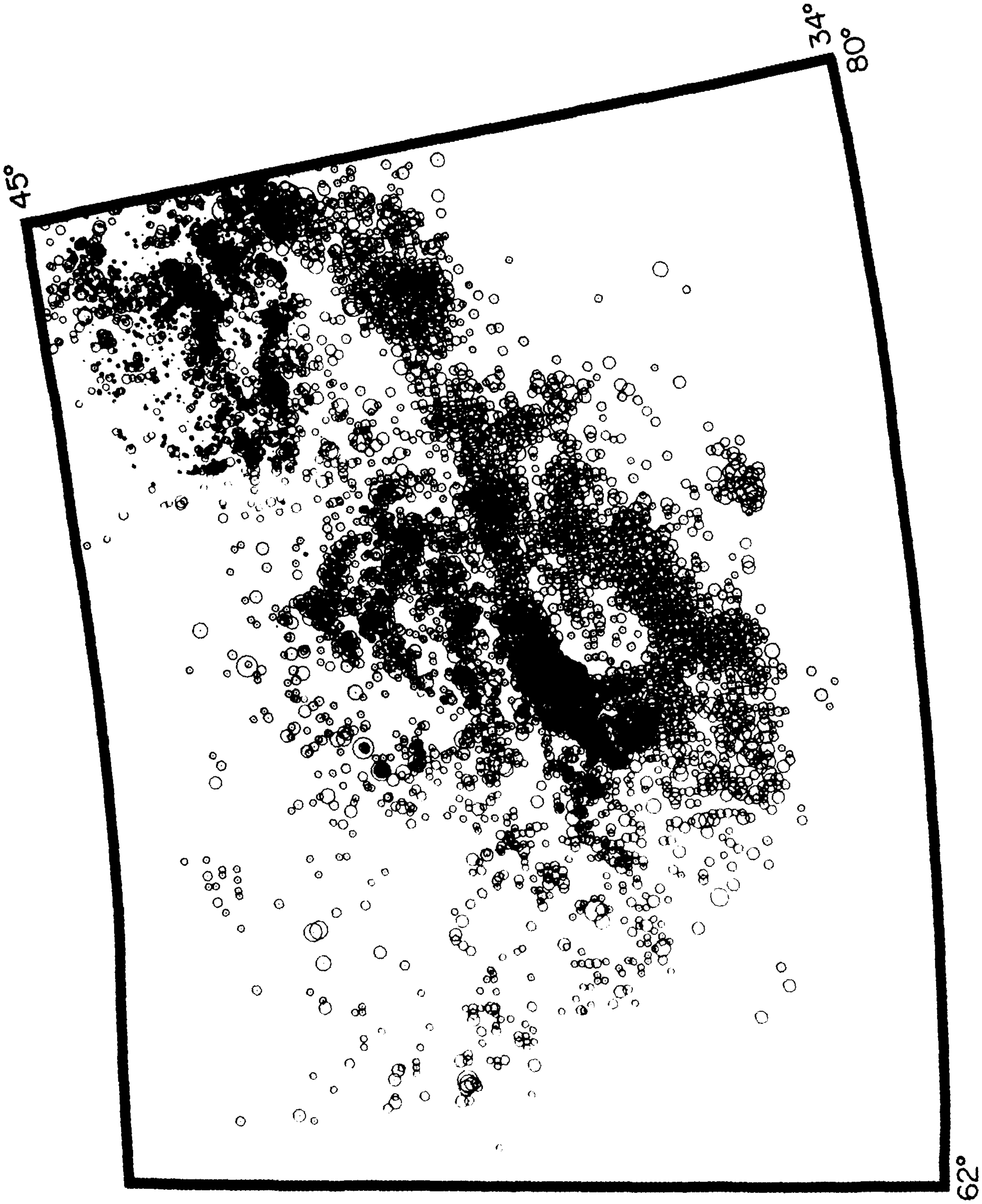

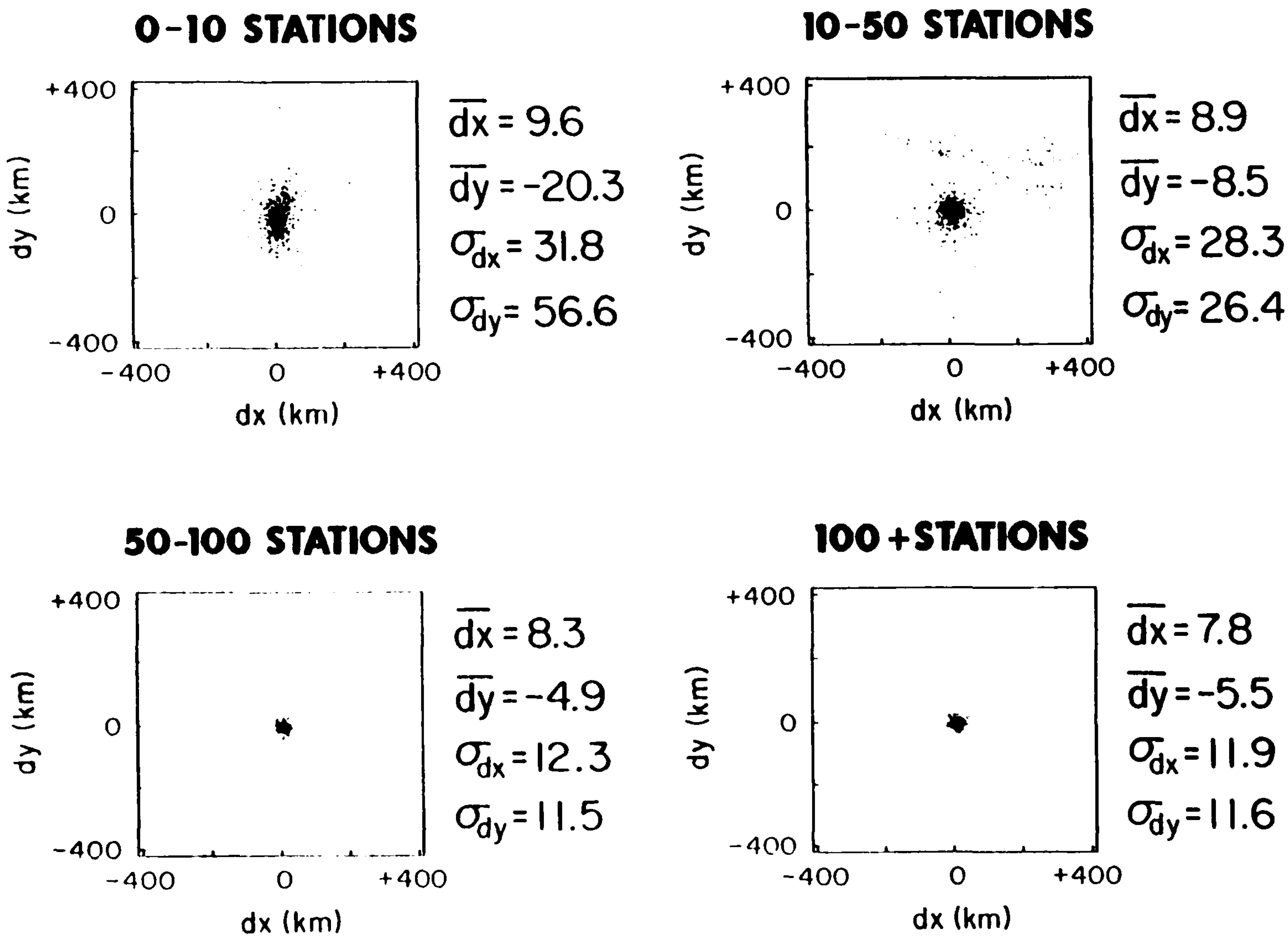

Figure 6 Difference in latitude and longitude (dy and dx) between ZSSSR location (origin in each graph) and ISC location for all earthquakes common to both catalogs, as a function of the number of stations used for location by ISC.

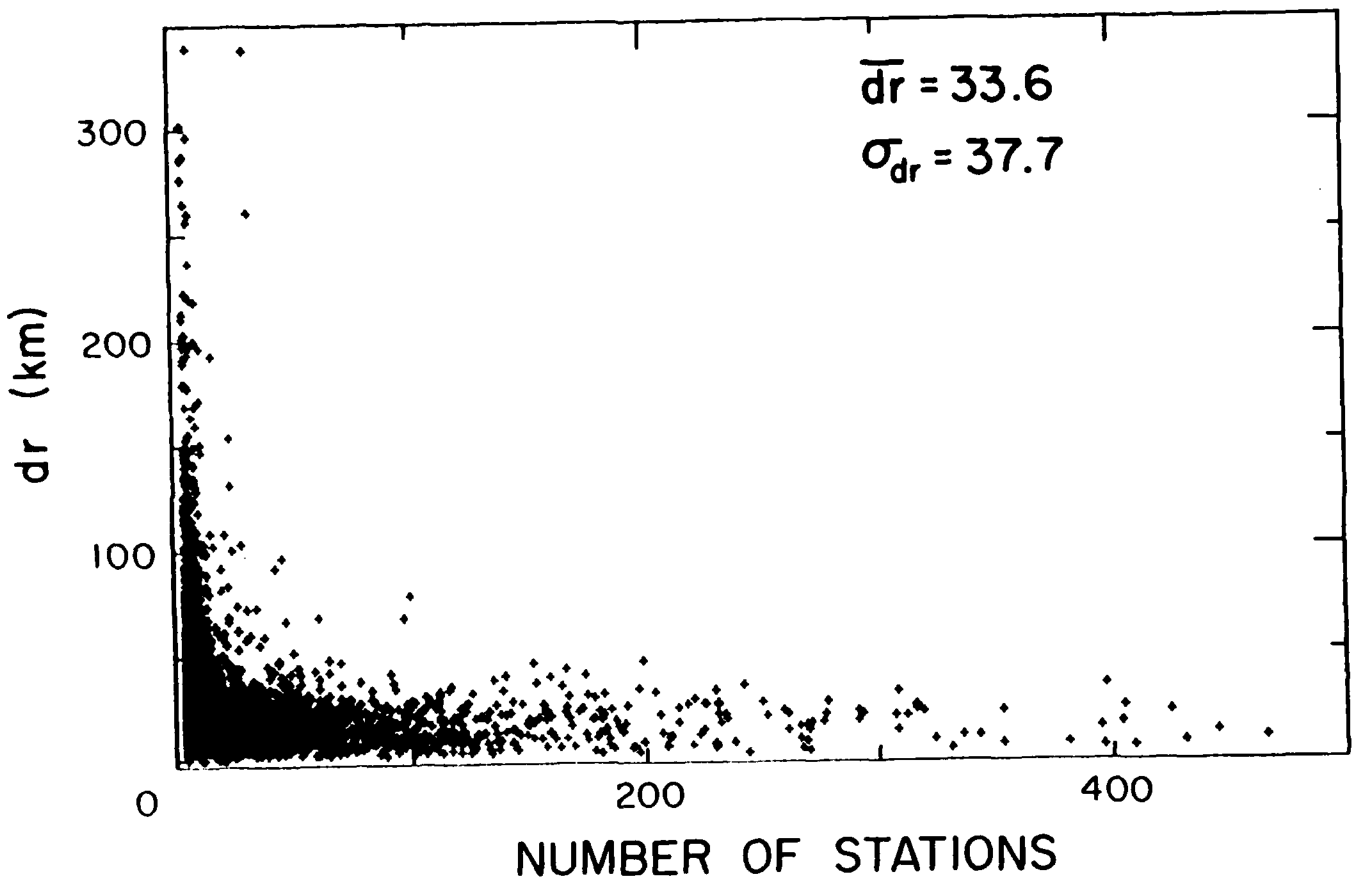

Figure 7 Difference in epicentral location (dr) between ISC and ZSSSR catalogs as a function of the number of stations used for location by ISC.

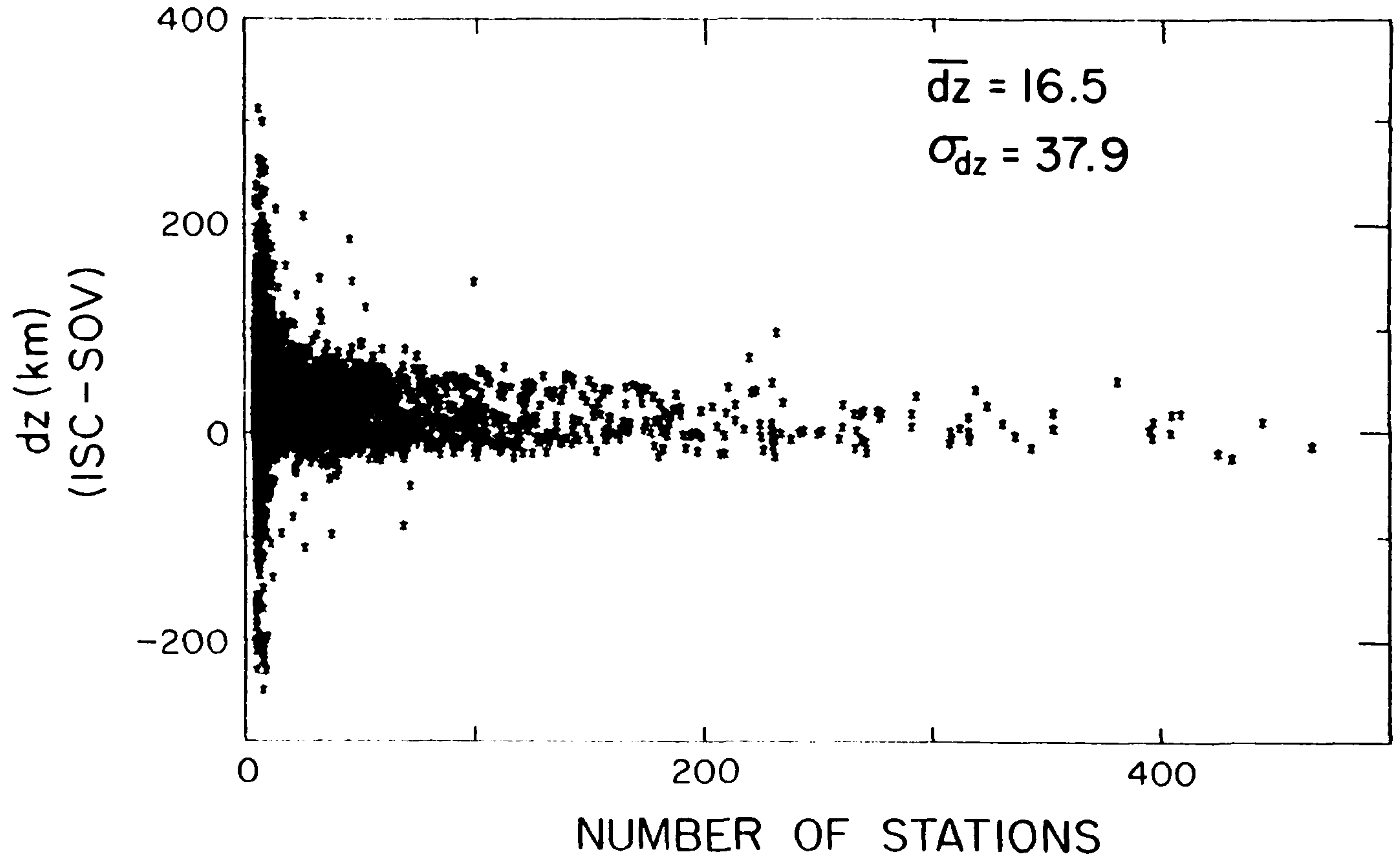

Figure 8 Difference in depth (dz) between ISC and ZSSSR catalogs as a function of the number of stations used for location by ISC.

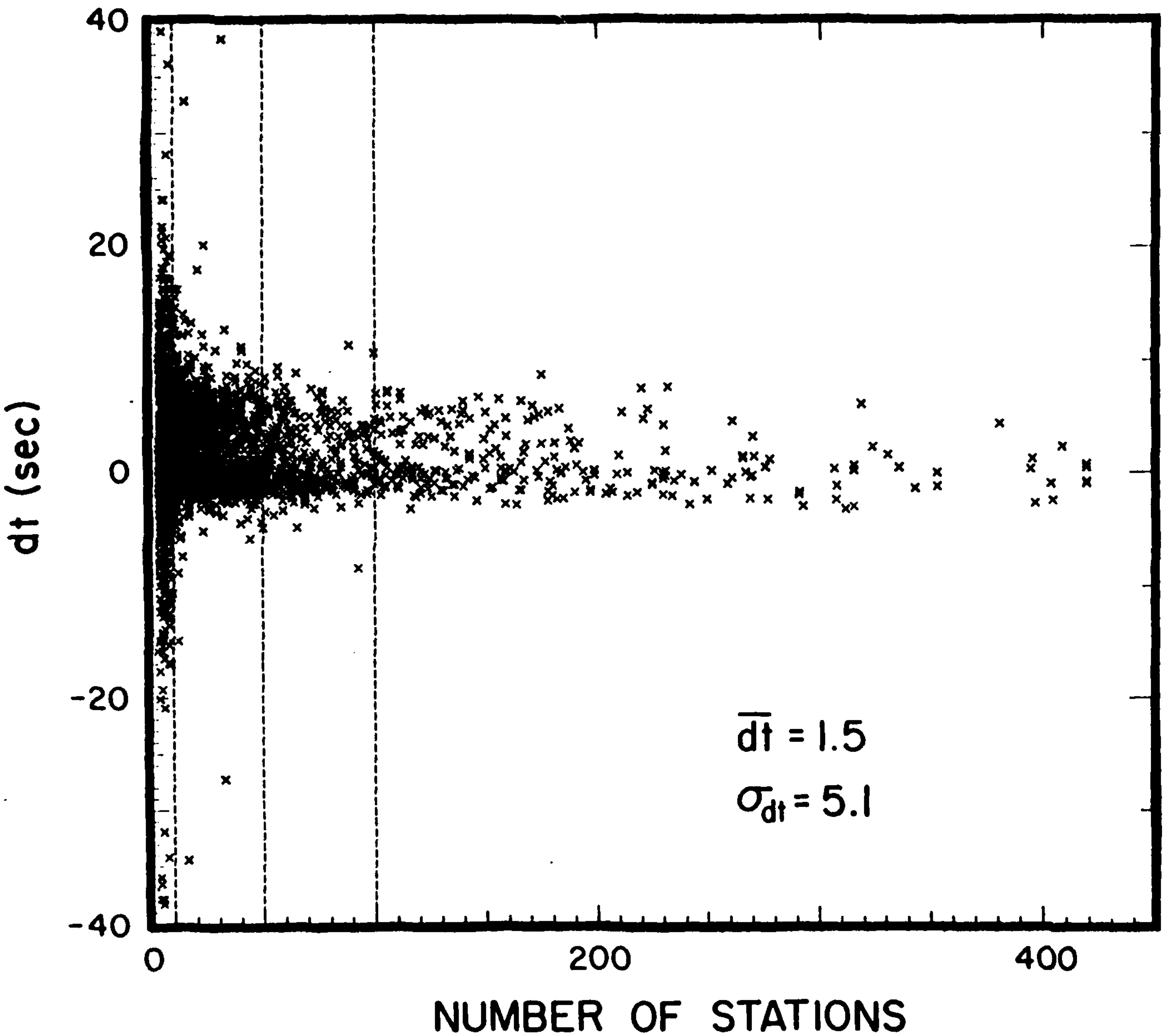

Figure 9 Difference in origin time (dt) between ISC and ZSSSR catalogs as a function of the number of stations used for location by ISC.

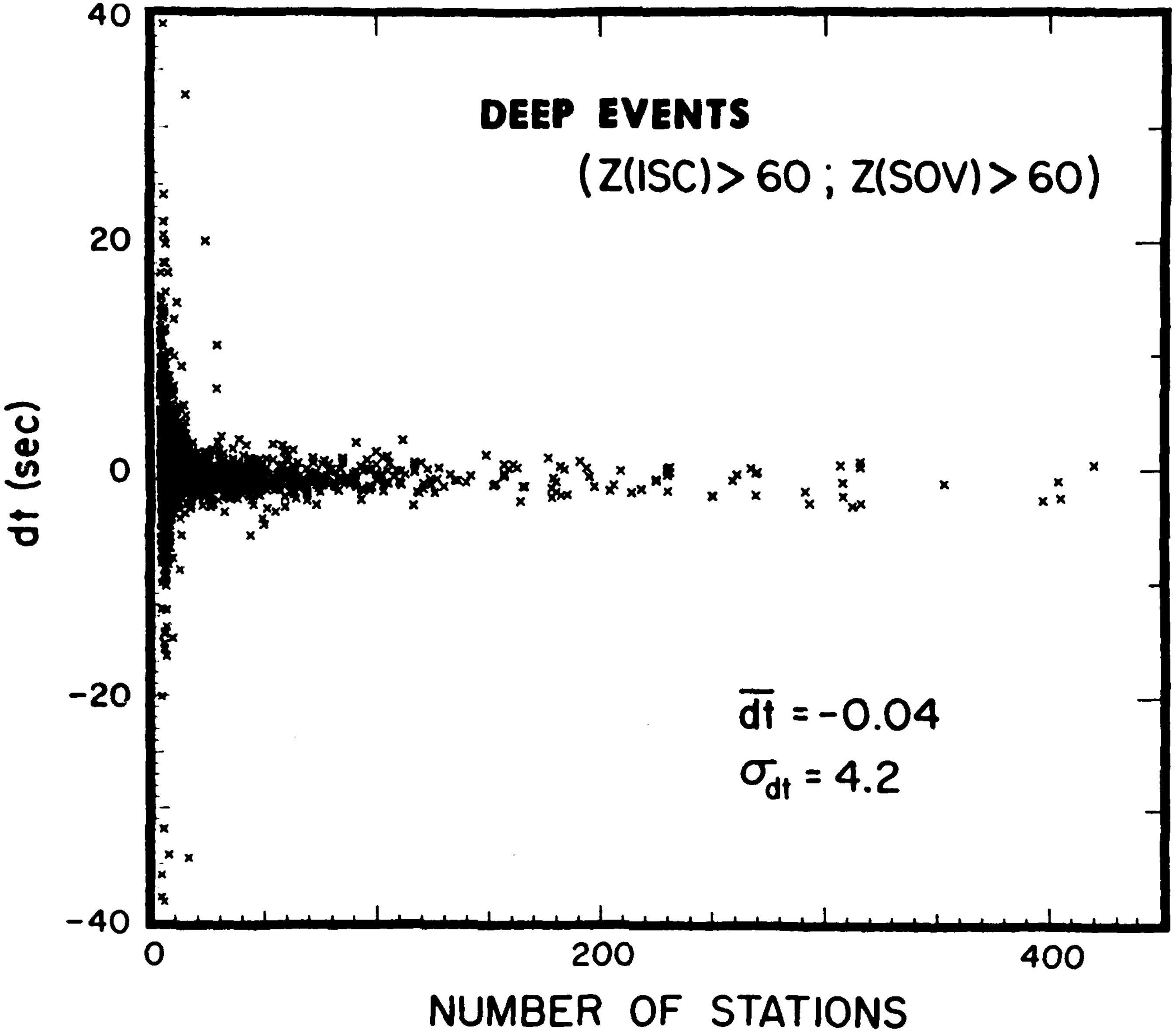

Figure 10 Difference in origin time (dt) between ISC and ZSSSR catalogs, as a function of the number of stations used for location by ISC, for deep events (those for which both the ZSSSR and ISC depths are greater than 60 km). (Note - positive dt is for ISC origin times later than ZSSSR).

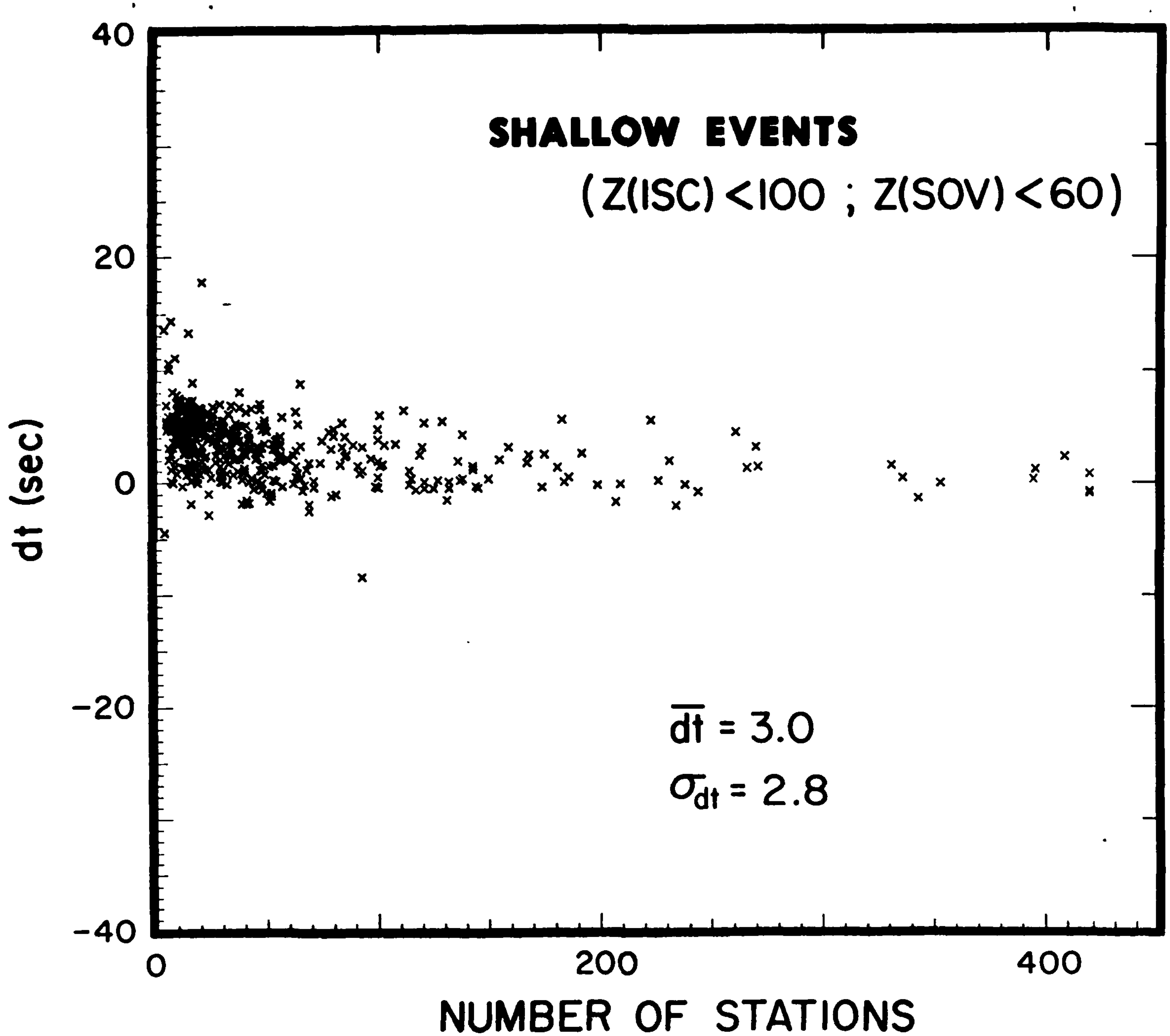

Figure 11 Same as Figure 10, but for shallow events (those for which the ZSSSR depth is less than 100 km and the ISC depth is less than 60 km, but neither are the default depths of 0 or 33 km).

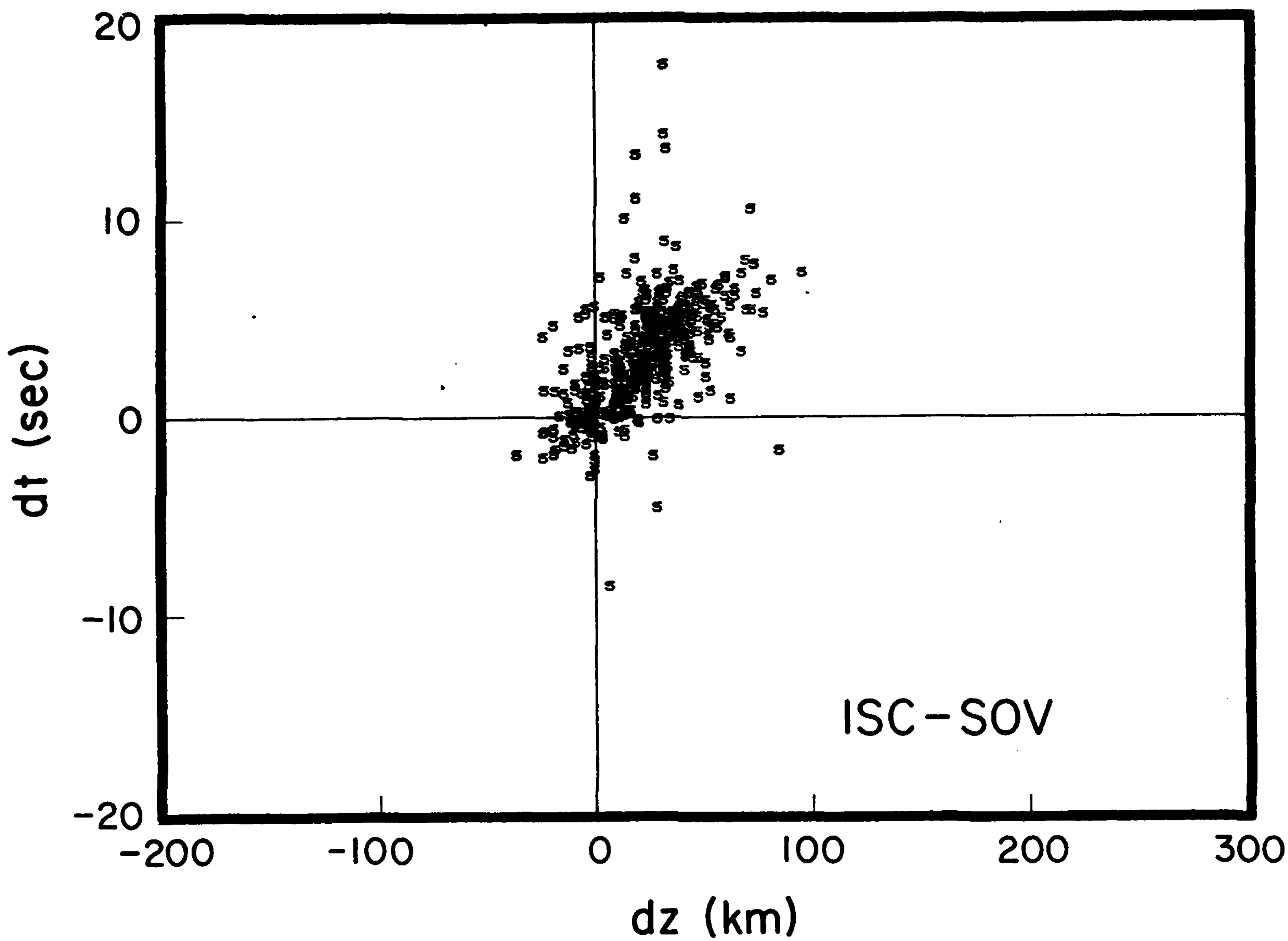

Figure 12 Difference in origin time (dt) vs difference in depth (dz) for shallow events (as defined in Figure 11).

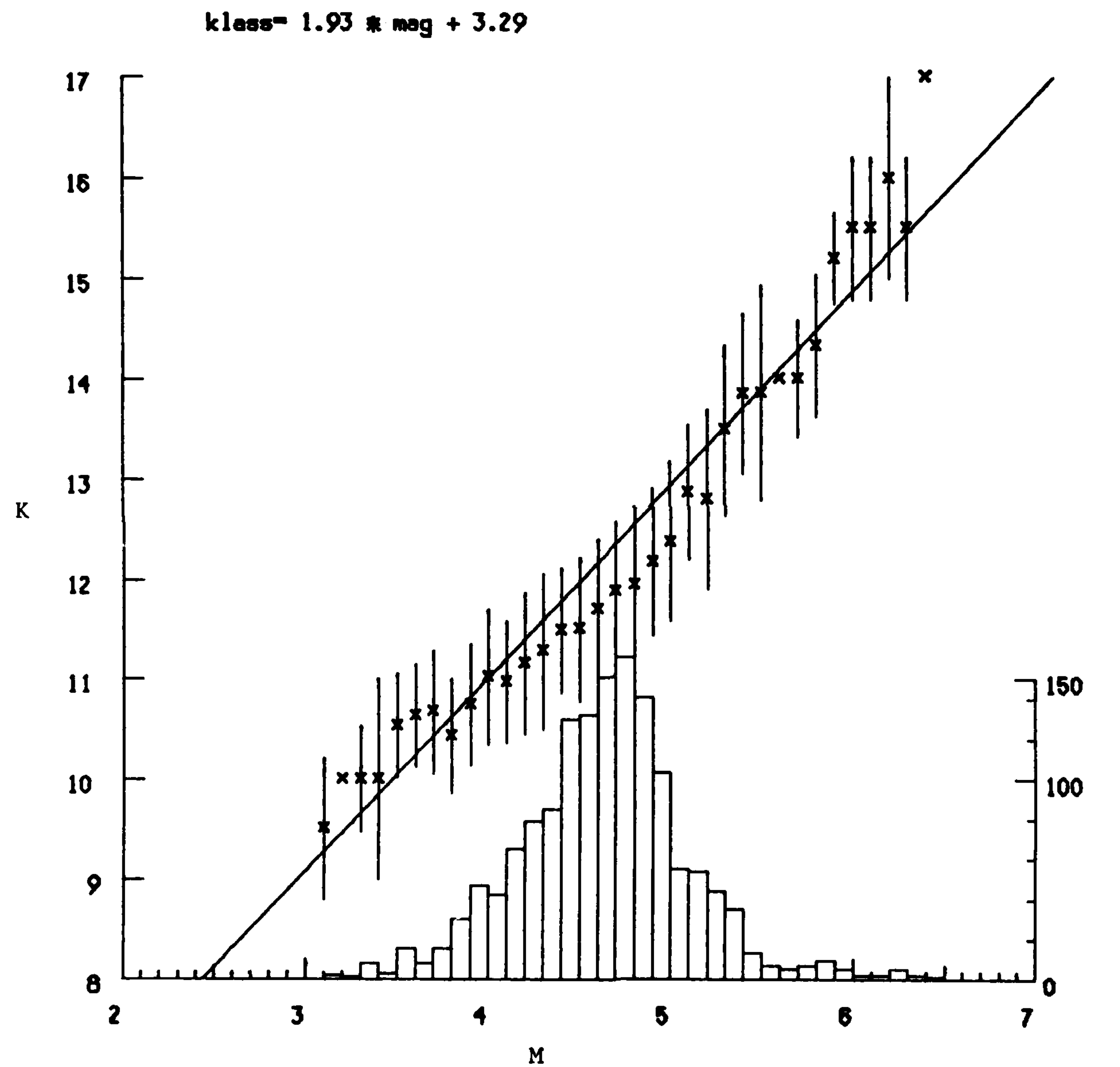

Figure 13 ZSSSR energy class (k) vs ISC magnitude (m_b) and number of earthquakes in ISC for each 0.1 magnitude increment. Least squares regression (with weight inversely proportional to square of the standard deviation of the average magnitude for each magnitude interval) is shown and compared to the standard formula of Rautian.

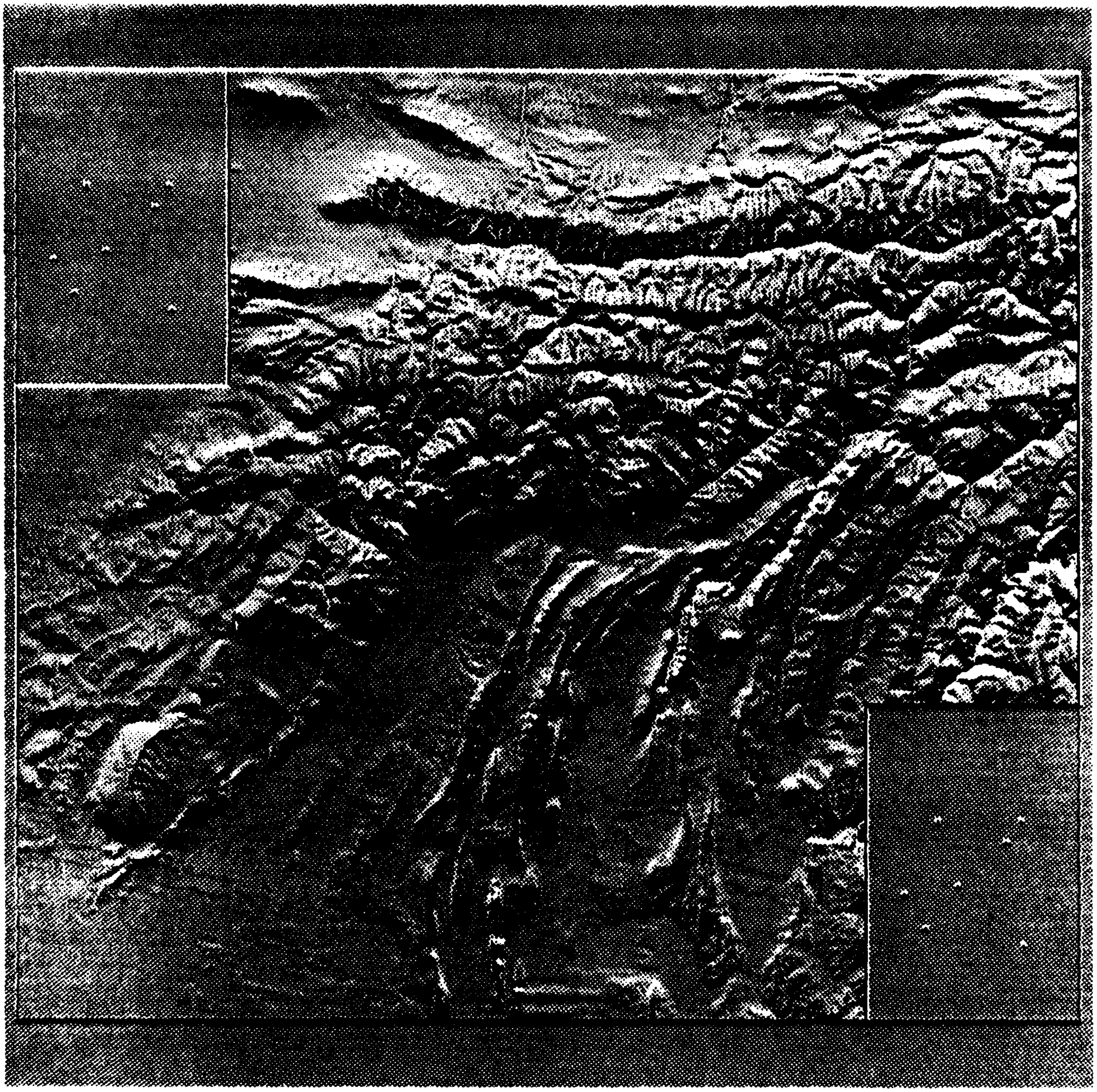

Figure 14 Topographic map of the Tadjik Depression and Southern Tien Shan created from DMA digital terrain data. Blanks in upper left and lower right are missing data. Geographic locations are indicated for comparison with other maps. Shading is for illumination from the north.

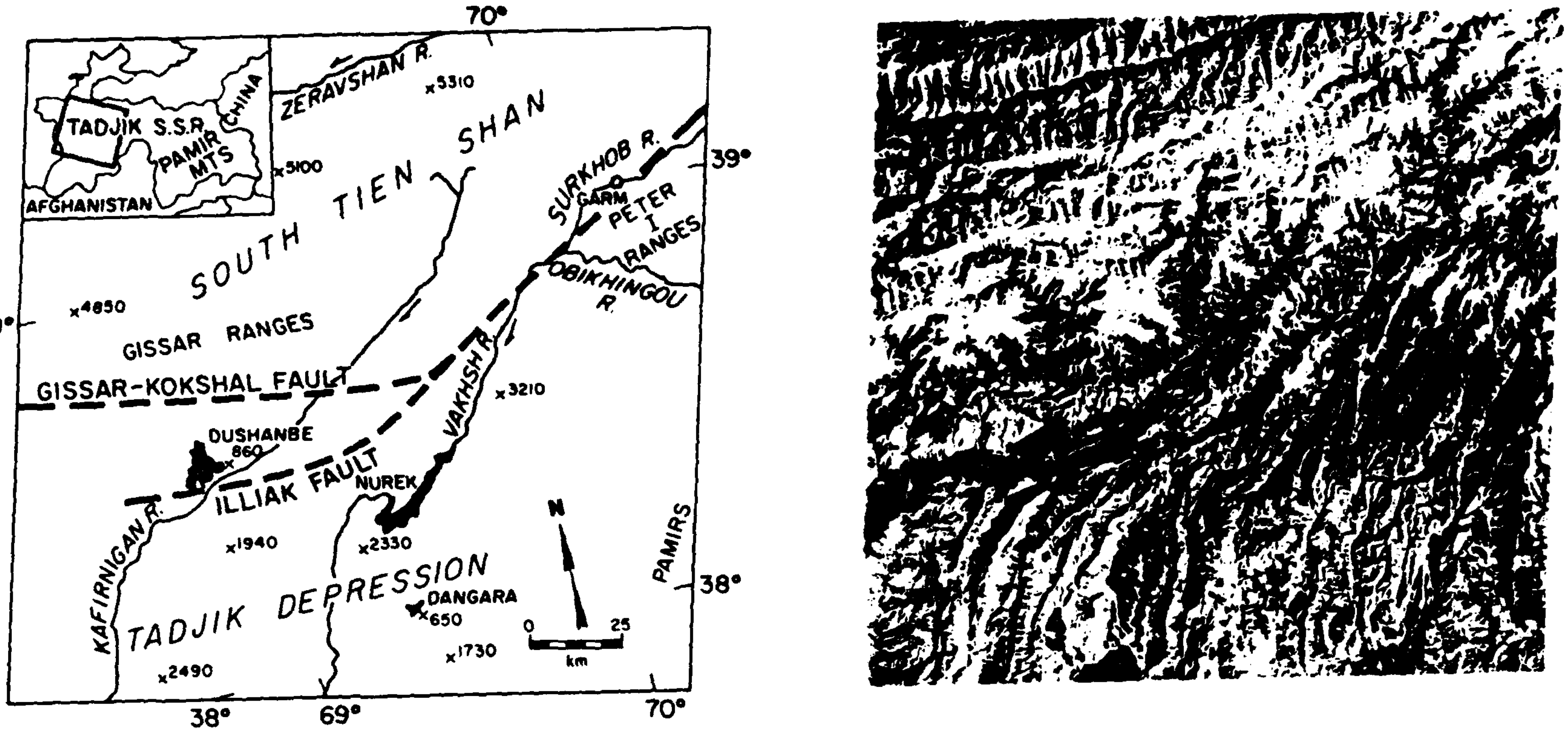

Figure 15 Landsat image (right) and location map (left) for a portion of the region shown in Figure 14 (from Simpson and Negmatullaev, 1981).

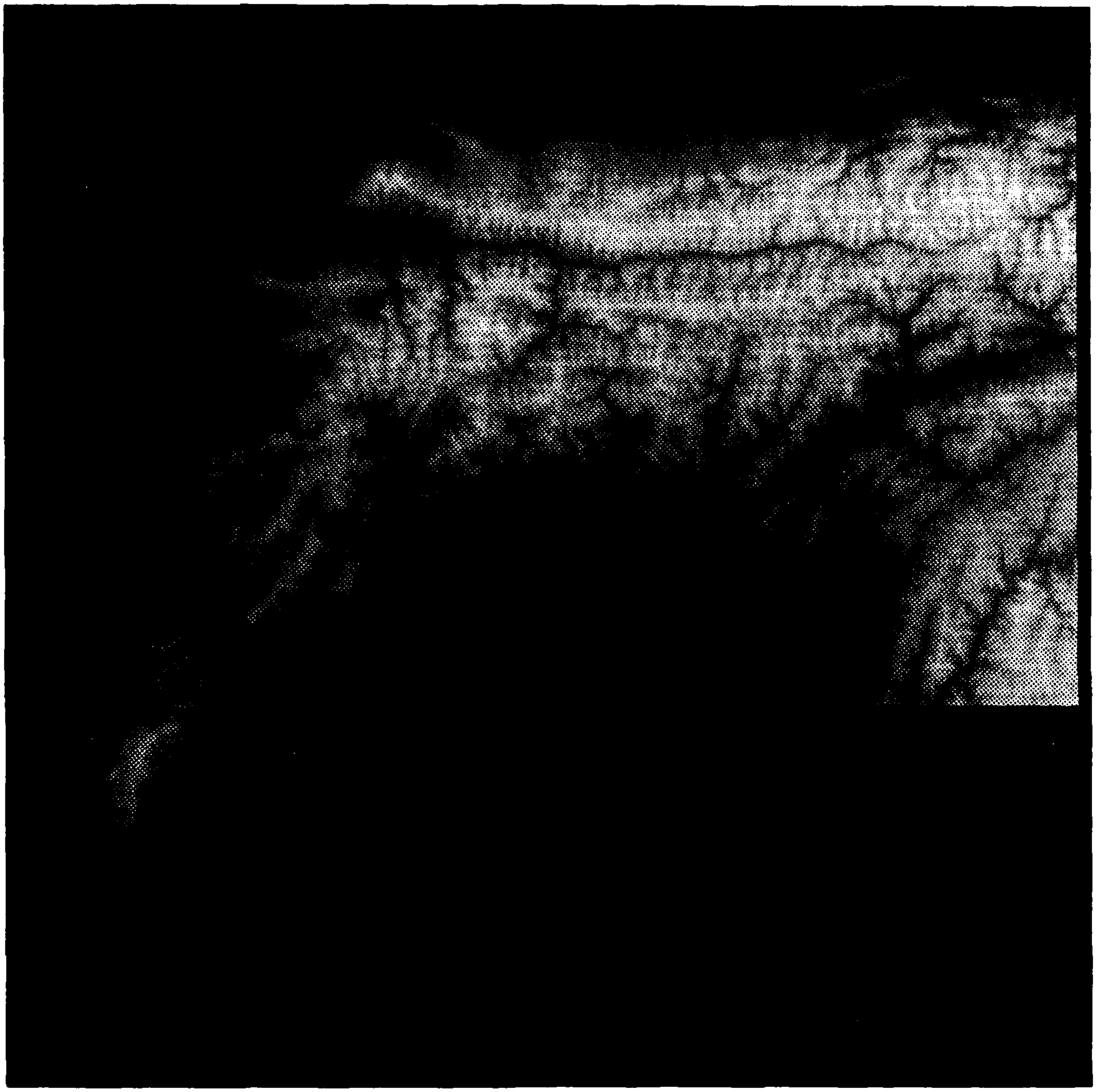

Figure 16 Raw digital terrain data with intensity proportional to elevation.

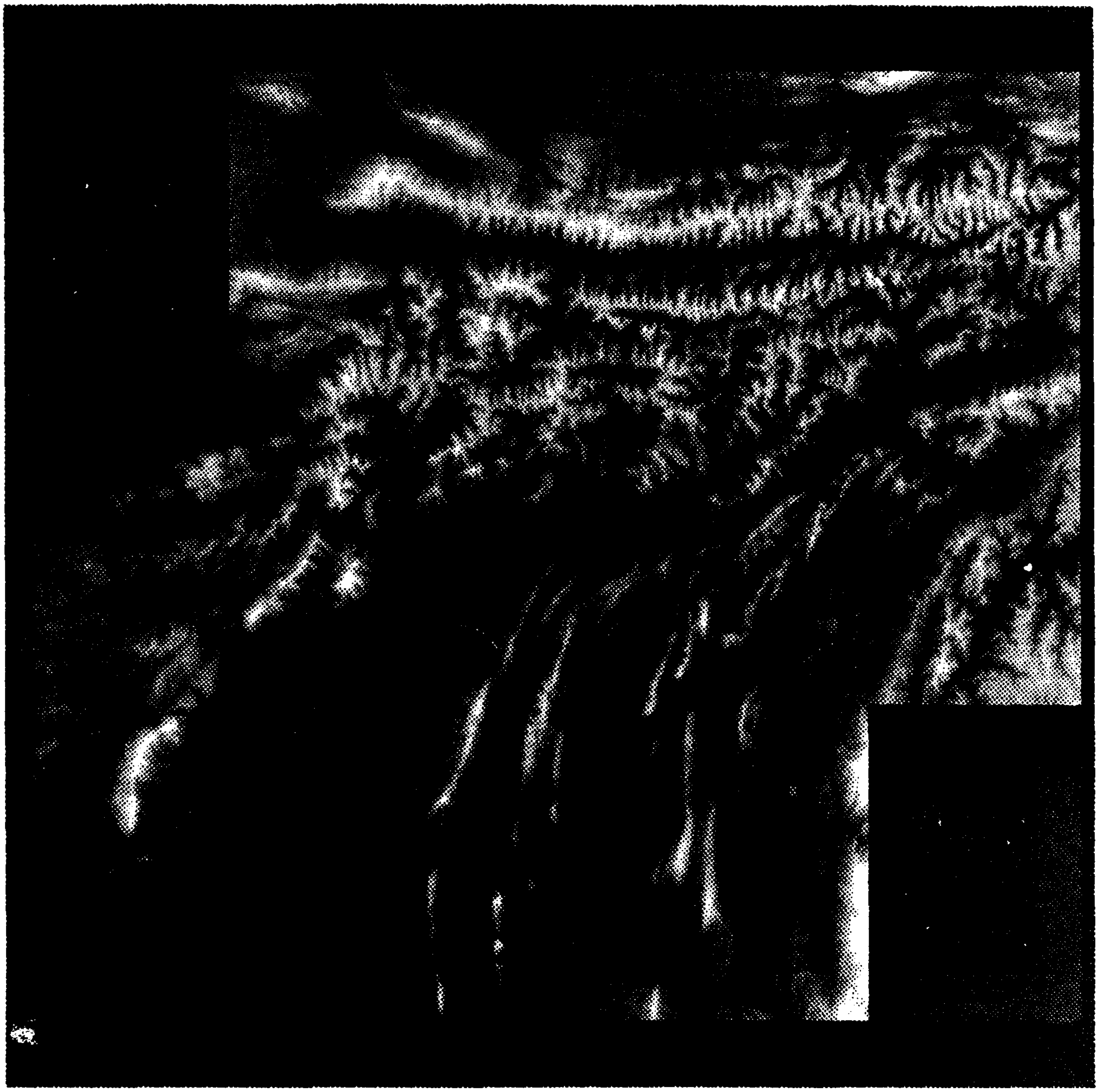

Figure 17 Terrain data with enhancement to locally adjust contast for higher resolution of small scale features.

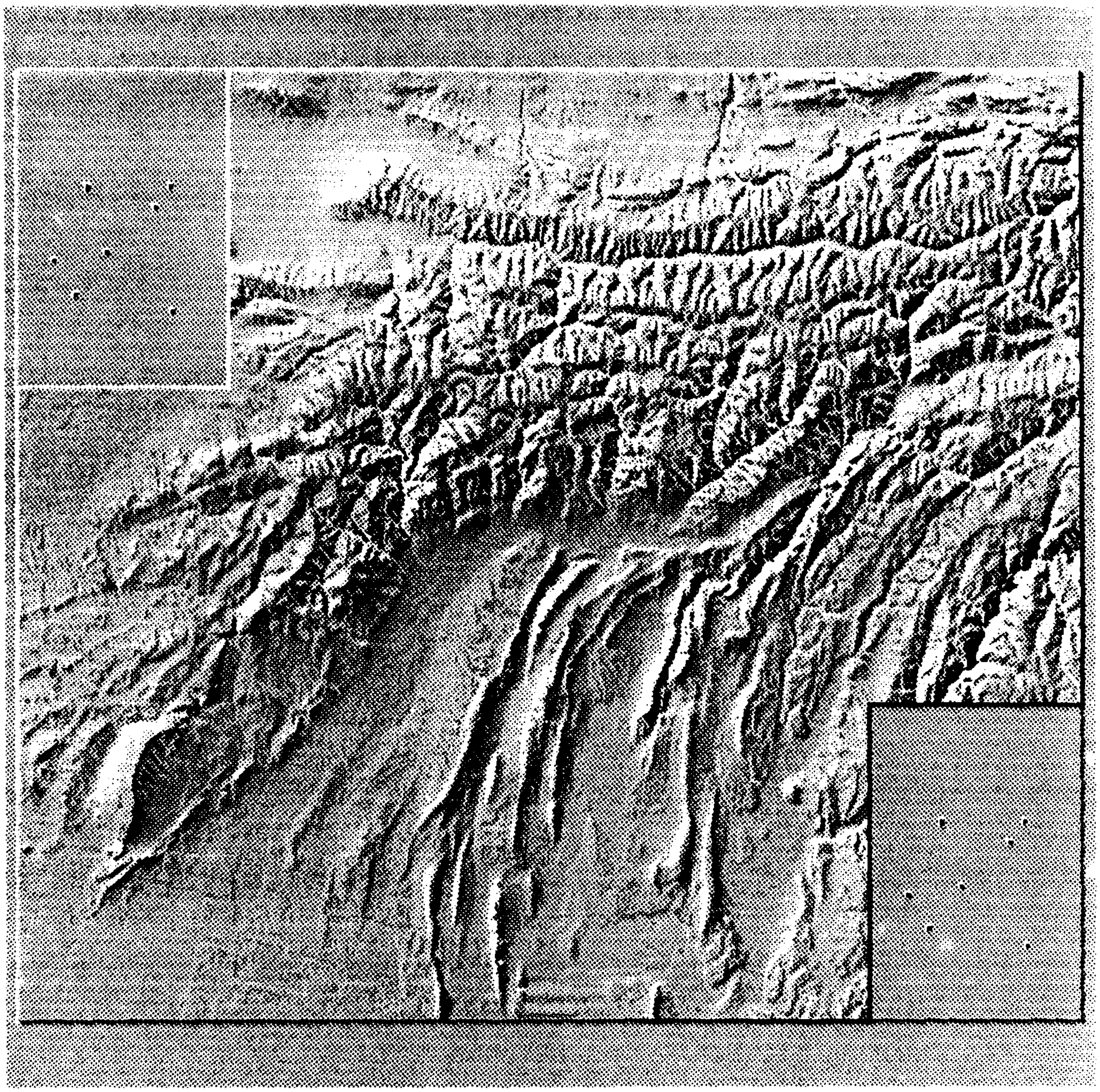

Figure 18 Shaded relief map with illumination from the northwest.

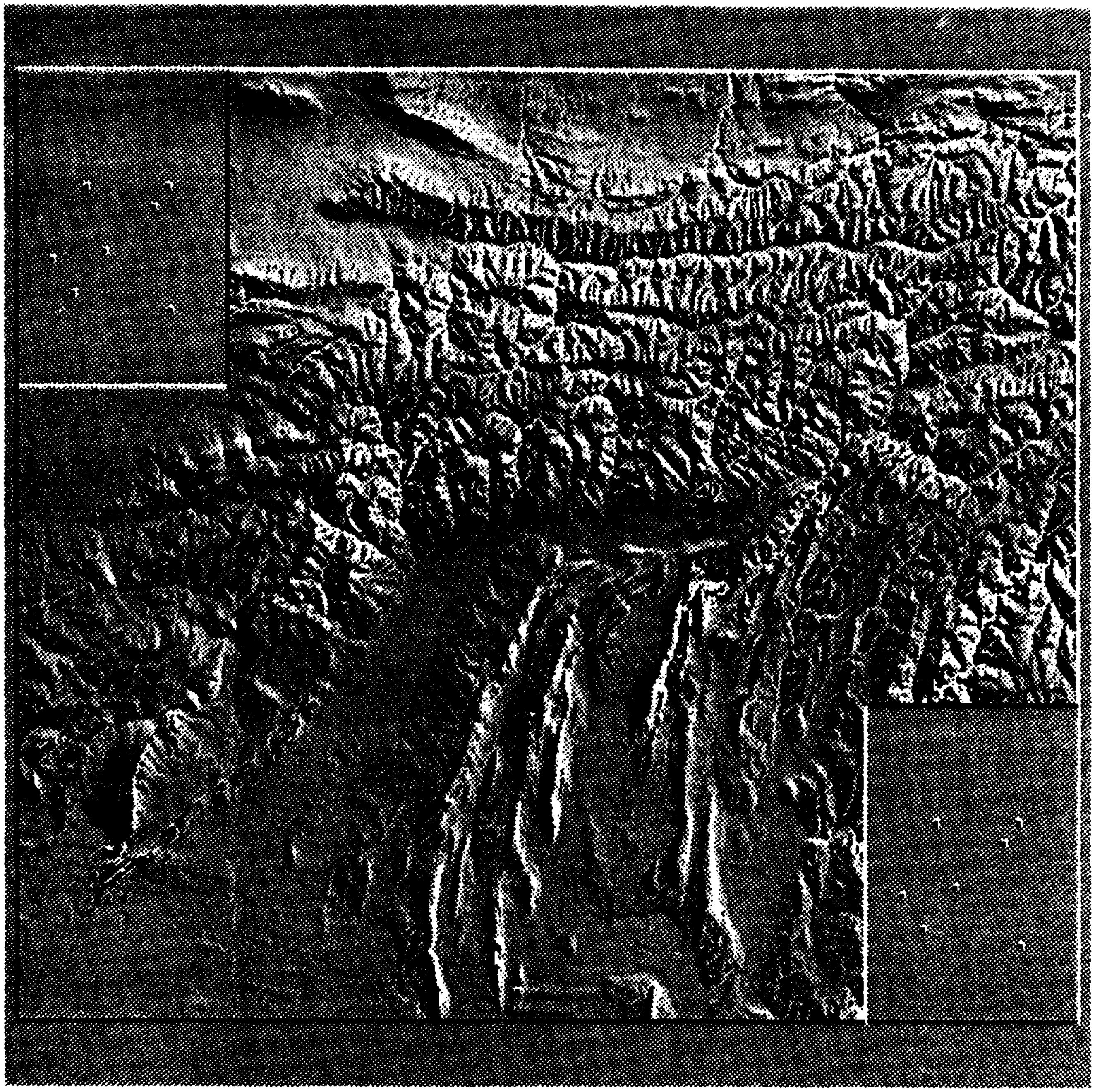

Figure 19 Shaded relief map with illumination from the northeast. Comparison with Figures 14 and 18, especially of river valleys in the northeast segment, shows how different gradient determinations (illumination directions) enhance features at different azimuths.

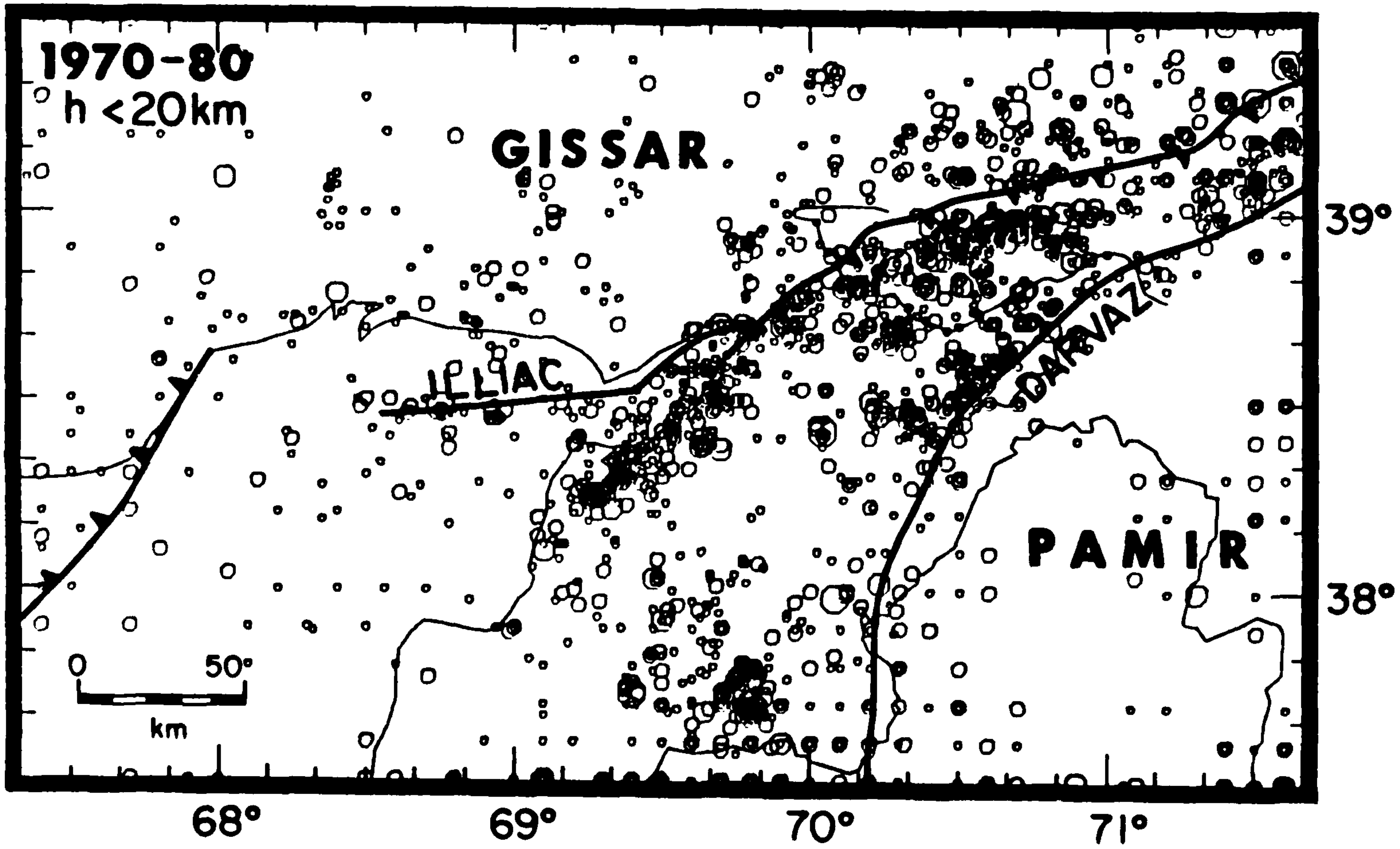

Figure 20 Seismicity of the Tadjik Depression and Gissar Kokshal seismic zones from the ZSSSR earthquake catalog for 1970-80. Kulyab seismicity is the cluster in the southern part of the map near 69°45' E.

Figure 22 Perspective view of the area show in Figure 21. Digital terrain data have been used to create a pespective image (viewed from the southwest) and the Landsat image has been registered with it to create surface texturing. The salt dome in the lower right stands more than 800 m above the surrounding valley.

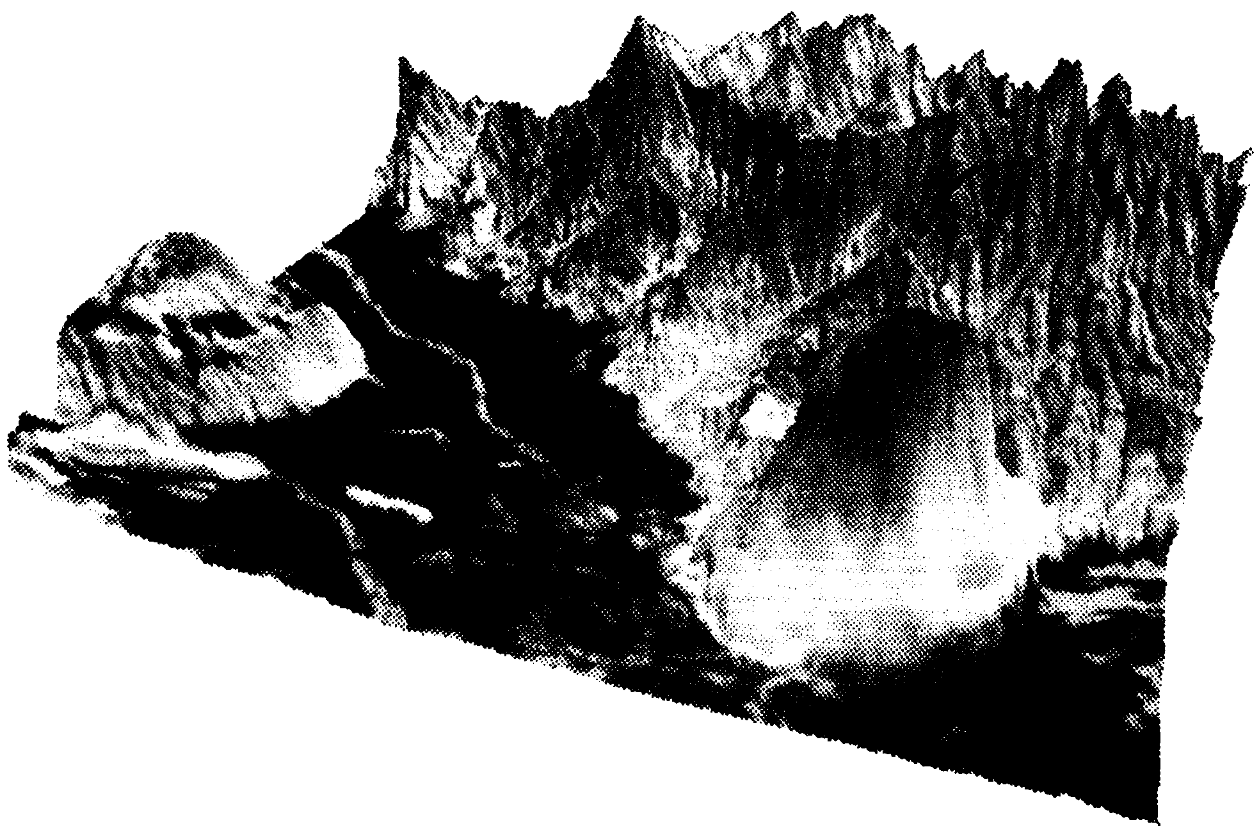

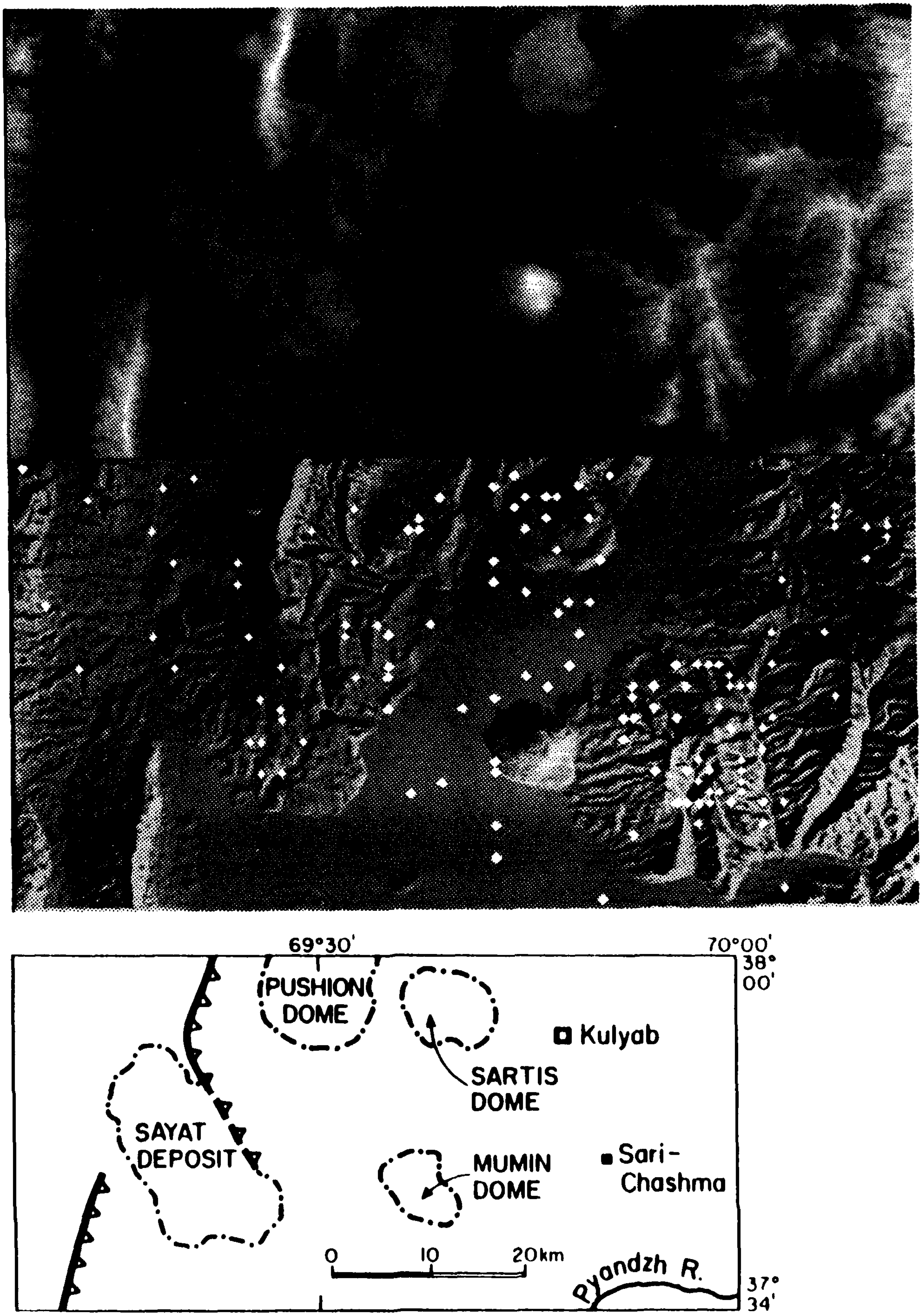

Figure 23 (top) Raw digital terrain data for the Kulyab area. (middle) Shaded relief map with seismicity superimposed. (bottom) Location map (from Leith and Simpson, 1986).

REFERENCES

Keith, C., D. W. Simpson, and O. Soboleva, Induced seismicity and deformation style at Nurek reservoir, Tadjik, SSR, J. Geophys. Res., 87, 4609-4624, 1982.

Kristy, M., and D. W. Simpson, Seismicity changes preceding two recent Central Asian earthquakes, J. Geophys. Res., 85, 4829-4837, 1980.

Leith, W., and W. Alvarez, Structure of the Vakhsh fold-and-thrust belt, Tadjik SSR: Geologic Mapping on a Landsat image base, Geol. Soc. Am. Bull., 96, 875-885, 1985.

Leith, W., and D. W. Simpson, Seismic domains within the Gissar Kokshal seismic zone, Soviet Central Asia, J. Geophys. Res., 91, 689-699, 1986a.

Leith, W., and D. W. Simpson, Earthquakes related to active salt doming near Kulyab, Tadjikistan, USSR, Geophys. Res. Lett., 13, 1019-1022, 1986b.

Leith, W., D. W. Simpson, and W. Alvarez, Structure and permeability: Geologic controls on induced seismicity at Nurek reservoir, Tadjikistan, USSR, Geology, 9, 440-444, 1981.

Rautian, T. G., Earthquake energy (in Russian), in Methods of Detailed Investigations of Seismicity, U. V. Riznishenko, ed., Academy of Sciences USSR, Moscow, pp. 75-113, 1960.

Simpson, D. W., and S. K. Negmatullaev, Induced seismicity at Nurek reservoir, Tadjikisan, USSR, Bull. Seismol. Soc. Am., 71, 1561-1586, 1981.

GEOPHYSICAL RESEARCH LETTERS, VOL. 13, NO. 10, PAGES 1019-1022, OCTOBER 1986

EARTHQUAKES RELATED TO ACTIVE SALT DOMING NEAR KULYAB, TADJIKISTAN, USSR

William Leith and David W. Simpson

The Lamont-Doherty Geological Observatory of Columbia University

Abstract. In the region near Kulyab, Tadjikistan, hundreds of shallow earthquakes with magnitudes greater than 2½ have been reported in Soviet yearly catalogs since 1964. This area appears as a well-defined cluster of activity, distant from the line of epicenters that defines the Gissar-Kokshal seismic zone, to the north of the Pamir ranges. The geology of this region is dominated by the presence of numerous salt domes, surrounded by Neogene and Quaternary continental deposits. The spatial relationship between these earthquakes and the salt domes suggests that the two phenomena may be related. Moderate earthquakes (M > 5) occurred in 1972 and 1973, and intensities of surface shaking greater than MM=6 were reported from earthquakes in 1937, 1952, 1969, 1972, 1973 and 1978. The earthquake on 2 April 1973 and its aftershocks were located in a region where no salt domes have been mapped at the surface. However, a buried salt diapir has been mapped at depth by geophysical means. These earthquakes may result from active salt diapirism at depth. The mechanism for producing this seismicity could be either the active fracturing of the cap rock by the rising diapir, or the concentration of tectonic stresses in the thinned section above and adjacent to the diapir. The salt-related earthquakes may produce lower frequency radiation than other events of the same size.

Introduction

Salt deposits, and specifically salt domes, are currently of special interest as possible sites for decoupling of underground nuclear explosions [Hannon, 1985], or for the underground storage of radioactive nuclear waste, petroleum or gas condensate [Cohen, 1977; Borg, 1983]. The relatively structureless, homogeneous nature of salt formations, combined with the high solubility of rock salt, lend these formations to the mining of the large stable cavities that would be required to decouple a small underground nuclear explosion. In contrast with bedded salt deposits, salt domes are considered ideal cavity sites because of their large vertical dimensions and relatively pure salt content. In terms of explosion decoupling and the detection of clandestine nuclear weapons tests, earthquakes that are spatially associated with salt domes pose the obvious problem of discrimination. In terms of engineering activities, either on the surface or within the salt dome, earthquakes represent a hazard to the stability of any cavity constructed. Also, as potential sites for hazardous waste or other liquid storage, they may affect the short-term permeability of the cavity walls.

There is an extensive literature on salt diapirism [e.g., Lerche, 1986]. Salt domes are produced by the post-depositional flow of bedded salt upward through the overlying rock formations, because of the gravity (density) instability inherent in buried salt. It is generally considered necessary for salt dome regions to have undergone some degree of tectonism (associated with sedimentary loading) in order for diapirs to develop. Therefore, the process of salt dome formation is unstable and episodic and the rates of salt dome uplift are highly variable, depending on both the tectonics of the region and the state of maturity of the diapir [Jackson and Talbot, 1986].

Salt is an extremely weak rock, and deforms ductilely at geological strain rates [Carter and Hansen, 1983]. Salt areas are generally not associated with earthquakes, and to date there is no literature associating earthquakes with active salt doming. Where studies have been made of the seismicity of salt dome areas in East Texas and the Gulf Coast [Dorman and others, 1977; Racine and Klouda, 1979], no definitive correlations between salt structures and earthquakes have been made. Nevertheless, sounds of salt movement have been detected in salt dome regions in Iran [Kent, 1979], and rock bursts have occurred in underground salt mines [see Baar, 1977]. Those salt dome areas where detailed seismicity studies have been made (east Texas, Louisiana, Oklahoma) are also areas where the domes are mature [Jackson and Talbot, 1986] and tectonic strain rates are low. Our study, from an area that is currently deforming at a relatively high rate, therefore contrasts with studies of the seismicity of salt dome areas in the U.S.

This letter describes the geological and seismological attributes of the Kulyab salt dome area, in the southwestern Tadjik SSR. The seismicity that marks this area stands out as a cluster of epicenters distinct from the main trend of the Gissar-Kokshal seismic zone (Figure 1), 50-100 km north of Kulyab [Leith and Simpson, 1986].

Geology

The Soviet republic of Tadjikistan is marked by an active tectonics and a high rate of natural seismicity. As part of the India-Asia collision, the Jurassic and younger sediments that fill the sedimentary basin of the Tadjik Depression, a relatively low region that forms most of southwest Tadjikistan (Figure 2), have been deformed by folding and thrusting in the zone between the Pamir and Tien Shan ranges.

Paper number 6L7011.
0094-8276/86/006L-7011$03.00

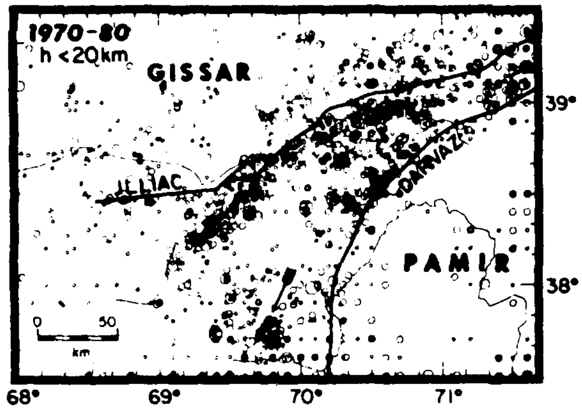

Fig. 1. Shallow earthquakes for the area of southwestern Tadjikistan from 1970-1980. Seismicity is most intense within the frontal (northern) portions of the Vakhsh fold/thrust belt and along a portion of the Darvaz fault. The cluster of seismicity in the lower portion of the figure (arrow) occurs near the salt domes mapped in Fig. 2, and well away from the belt of epicenters that marks the fold/thrust belt. A detail of this area is shown in Fig. 3.

Throughout the Depression, Jurassic evaporites form the base of the sections exposed along thrust faults at the surface, and the overall structure of the Depression suggests that these basal evaporites form the decollement across which the thrusts are displaced [Leith and Alvarez, 1986]. Basin formation in mid-Jurassic time was followed by the deposition of large thicknesses of evaporites. Since the end of the Jurassic, shallow-water marine sedimentation in the Depression proceeded at a relatively slow rate, as the basin subsided following the rifting event [Leith,

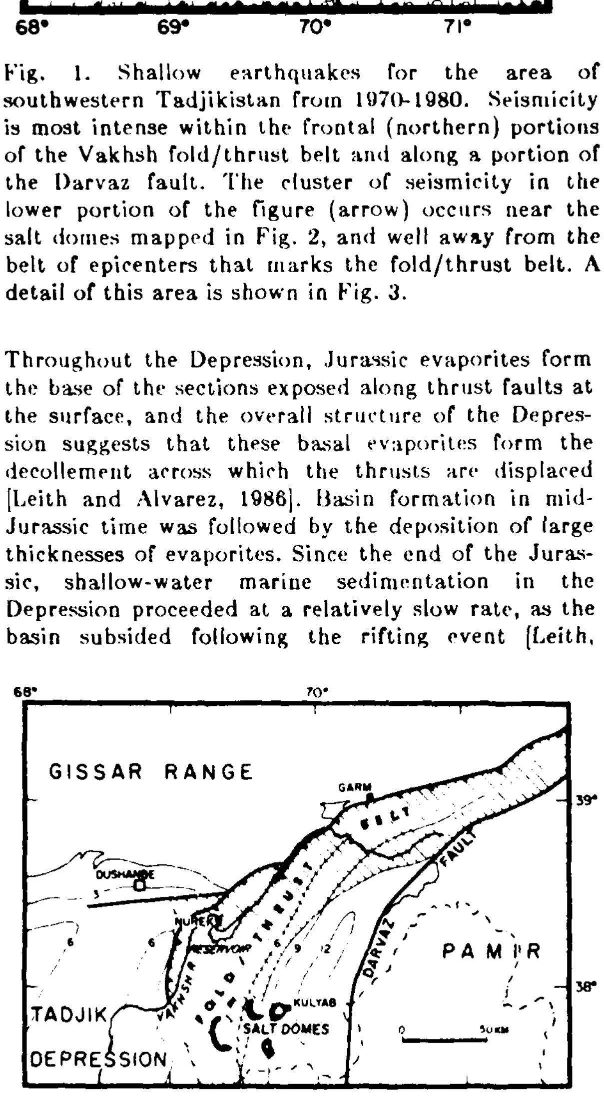

Fig. 2. Generalized crustal structure and geology of the northern Tadjik Depression. Salt domes are located near Kulyab in the southeastern Tadjik Depression, 10-50 km from the Soviet-Afghan border, which follows the Pyandzh river (dash-dot line). Depth to basement beneath the Mesozoic and Cenozoic sediments of the Tadjik Depression is contoured in 3 km intervals (thin lines).

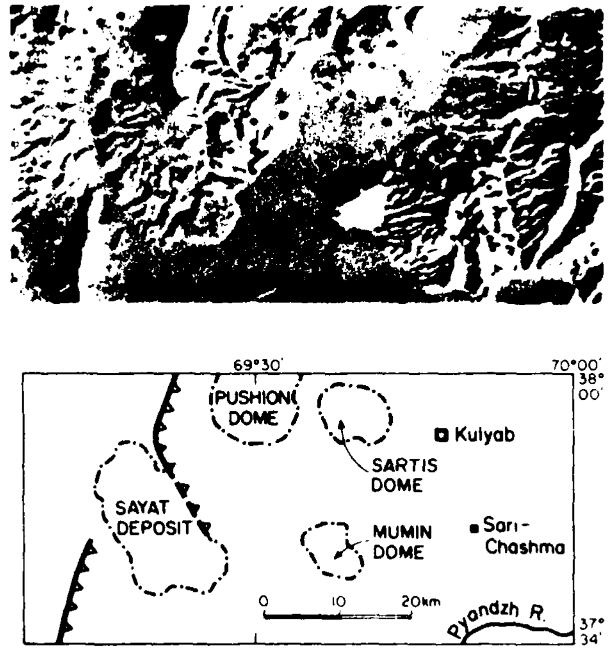

Fig. 3. (*a*) Earthquake epicenters from the Soviet Catalogs for the Kulyab region, mapped on shaded digital terrain data. (*b*) Sketch shows salt deposits, major faults and geography. There is a close spatial correlation between some groups of *earthquakes* and mapped salt domes. The cluster of earthquakes in the lower right is associated with the buried Sari Chashma salt diapir (detail in Fig. 4). Location accuracy for most events is listed as $\pm$ *10 km*.

1985]. Adjacent to the Pamir range in the region of Kulyab, this was followed in about middle Oligocene time by the deposition of more than 8 km of Neogene molasse in a north-south trending trough of thick and, now, gently-folded rocks (the Kulyab synclinorium). This rapid loading of the Jurassic-Paleogene section has provided the drive for the salt migration.

The Kulyab area, along the western limb of the Kulyab synclinorium, is marked by the outcrop of several large bodies of Jurassic-Lower Cretaceous salt [Luchnikov, 1982]. Some are obvious domes (Figure 3), while others mark the traces of mapped thrust faults. Several of the domes have prominent topographic relief. For example, at the Mumin dome, south of Kulyab (see Figures 3, 4), the central salt stock rises more than 870 m above the surrounding plain. This feeds an oblate glacial salt flow above folded and faulted upper Tertiary strata [Sadikov, 1982].

Geophysical studies and exploratory drilling that have accompanied the search for oil and gas in the Kulyab area have helped to delineate the distribution of salt at depth [Luchnikov, 1982; Azimov and others, 1982], and have enabled the mapping of a zone of overpressured formations to the west of Kulyab [Kalomazov and Vakhtikov, 1975]. A well drilled in the northern dome in Figure 3 ("Sartis") encountered

Fig. 4. Epicenters from the April 2nd, 1973 earthquake and its aftershocks, mapped on a Landsat image of the Kulyab area. The location of a mapped subsurface diapir (dashed line) is from Kon'kov [1974]. This earthquake sequence apparently occurred at shallow depth along the northern margin of the diapir.

pressures of 1.6 and 1.8 times hydrostatic in Turonian age strata at depths of 2642 and 2695 m, respectively. In general, the westernmost (up-structure) fields are overpressured (up to twice hydrostatic) while those to the east are not.

Seismicity

Epicenters of earthquakes in the Kulyab area from 1964-1980, from the yearly catalogs, Zemletracenniye v SSSR (hereafter, 'ZSSSR catalogs'), are shown in Figure 3, along with shaded digital topography. There are 352 earthquakes listed in the catalogs (many duplicate locations do not appear in the figure), all with magnitudes greater than about 2.5. All earthquakes in this area are shallow (< 20 km), and there is a clear association of some events with the mapped salt domes. The large cluster of activity in the lower right corner of the figure occurred following the M=5.2 earthquake on 02 April 1973 (hereafter, "1973 earthquake"). This sequence is associated with a diapir at depth, discussed below.

(A Soviet regional catalog lists some smaller events for the Kulyab area (to M < 2) but is incomplete. A map showing some smaller events was published in the 1979 ZSSSR catalog (p. 30 overleaf), but we cannot specify location accuracy and salt structures are not located on the map).

For the region of Figure 3, the b-value is approximately 1.1-1.2 for earthquakes from 1964-1980. This is relatively high in comparison with the western portion of the Vakhsh fold/thrust belt, and is, in fact, comparable to that of the reservoir-induced seismicity at Nurek [Simpson and Negmatullaev, 1981]. Induced earthquakes are triggered by effective stress changes resulting from changes in the subsurface pore pressure regime [Simpson, 1986], and relatively high b-values are typical of induced seismic activity [Gupta and Rastogi, 1976]. We suggest that the high b-value that we have determined for the Kulyab region may be "normal" for that area, because of the existence of the naturally high formation pressures noted above. The high b-values may thus be a fluid pressure effect that distinguishes this region from other areas in western Tadjikistan.

The Kulyab area has produced several earthquakes with magnitudes of about 5 in this century [Gubin, 1960], including those in 1937, 1952, 1959, 1972, 1973 and 1978. From these, the April 2nd, 1973 earthquake (M=5.2) is the best studied to date. Kon'kov [1974] combined data from the Kulyab seismic station with macroseismic data to relocate the epicenter of the main shock, which lies 15 km NNW of the epicenter reported in ZSSSR, at a depth of 12 km. It lies near the northern edge of the buried Sari-Chashma diapir, 10 km SE of Kulyab. The sequence is plotted with geologic and geographic data in Figure 4. The earthquakes apparently occurred along the northern margin of the Sari-Chashma diapir, at depths from 0 to 10 km. The main event (April 2, 00h02m43s) was included in a spectral study of Central Asian earthquakes by Zapol'skiy and Loginova [1984; figure 2], which suggests that this event produced lower frequency seismic waves than other earthquakes of comparable size. Low frequency microearthquakes near Nurek reservoir may also be associated with salt deposits, but more work needs to be done to determine the cause of the spectral anomaly.

Discussion

Salt diapirism in active tectonic regions can be associated with very high rates of deformation. It is therefore more appropriate to compare the dynamics of the Kulyab salt domes with those of the active salt dome area of southern Iran [Ala, 1974], rather than the more stable region of extensive salt domes along the U.S. coast of the Gulf of Mexico. For example, a detailed study of salt dynamics has been made for the Kuh-e-Namak intrusion in Iran [Talbot and Jarvis, 1984]. This salt stock *maintains* the highest known natural rate of salt extrusion, estimated by Talbot and Jarvis [1984] to average 170 mm/yr (or about 1 km/6000 yr). This represents an extremely high strain rate in the salt stock, and a significant additional shear stress in the adjacent country rock [D. Davis, pers. comm., 1986].

Because of the very active nature of the tectonics of Tadjikistan, we suspect that the diapirs near Kulyab reflect the same high degree of activity as the Iranian intrusions. For comparison, the *Mumin dome* (which is more than 7 km wide and rises more than 870 m above the adjacent alluvial plain; see Fig. 4) is

approximately the same size as the Kuh-e-Namak intrusion, and the domes are both in similar arid environments. The Mumin dome must, therefore, maintain a rate of salt extrusion of the order of the Kuh-e-Namak, in order to maintain comparable topography. Unfortunately, data on the deep structure of the Sari Chashma diapir or surface strains in the local area of the diapir are unavailable. Thus, we are currently not able to determine the amount or character of the deformation that is associated with the growth of this salt body.

Elsewhere in the Tadjik Depression, shallow seismicity is largely confined to the sedimentary section above the salt-layer decollement [Leith and Simpson, 1986], and salt is generally thought too weak to hold the large elastic strains that would be necessary to produce a moderate-size earthquake. Thus, we suspect that the 1974 earthquake sequence reflects fracturing of the country rock above or adjacent to the Sari Chashma diapir, and not the seismic release of stored elastic strains within the salt itself. However, depths and focal mechanisms of earthquakes in the Kulyab area are poorly constrained, and we must await further data before speculating on the mechanics of the deformation.

Acknowledgements. We thank L. Sykes, D. Davis and J. Rachlin for reviewing the manuscript, and J. Lewkowicz and DARPA for providing the digital terrain data for this region. This work was supported by DARPA/AFGL under contract F19628-85-K-0022 and by USGS contract G14080001-1168. Lamont-Doherty Geological Observatory contribution 4041.

References

Ala, M. H., Salt diapirism in southern Iran, *Am. Assoc. Petrol Geol. Bull 58*, 1758-1770, 1978.

Azimov, P. K., Ye. V. Lebzi and Yu. M. Ovchinnikov, 1982, Deep structure and problems of completion of the sub-salt sediments of southwest Tadjikistan, *Neftegazovaya Geol. i Geofiz 3*, 23-27.

Baar, C. A., *Applied Salt Rock Mechanics 1. The in situ Behavior of Salt Rocks*, 294 pp., Elsevier, Amsterdam, 1977.

Borg, I., Peaceful nuclear explosions in Soviet gas condensate fields, in *Energy and Technol. Rev.*, pp. 30-37, Lawrence Livermore Nat. Lab., 1983.

Carter, N. L. and F. D. Hansen, Creep of rocksalt, *Tectonophysics 92*, 275-333, 1983.

Cohen, B. L., The disposal of radioactive wastes from fission reactors, *Sci. Am. 236*, 21-31, 1977.

Dorman, J., G. V. Latham, J. L. Worzel and D. Dumas, Geophysical investigations of salt at the University of Texas geophysics laboratory, in *Proc. Conf. Salt Dome Utilization and Environmental Considerations*, Inst. Environ. Sci. Louis. St. Univ., p. 333-351, 1977.

Gubin, I. Ye., *Patterns of Seismic Activity in Tadjikistan*, 450 pp., Acad. Sci. Tadjikistan, Dushanbe, 1960

Gupta, H. K. and B. K. Rastogi, *Dams and Earthquakes*, 229 pp., Elsevier, Amsterdam, 1976.

Hannon, W. J., Seismic verification of a comprehensive test ban, *Science 227*, 251-257, 1985.

Jackson, M. P. A. and C. J. Talbot, External shapes, strain rates and dynamics of salt structures, *Bull Geol. Soc. Am. 97*, 305-323, 1986.

Kalomazov, R. U. and M. A. Vakhtikov, Appearance and Nature of anomalously high formation pressures in the Kulyab megasyncline of the Tadjik Depression, *Neftegazovaya Geologiya i Geofizika 10*, 3-6, 1975.

Kent, P. E., The emergent salt plugs of southern Iran, *J. Petrol. Geol. 2*, 117-144, 1979.

Kon'kov, A. A., The Kulyab earthquake of 2 April, 1973,in *Zemletryacennii v SSSR v 1973 Godu*, edited by I.V. Gorbunova and others, p. 86-93, Nauka, Moscow, 1976.

Leith, W., A Mid-Mesozoic extension across Central Asia?, *Nature 313*, 567-570, 1985.

Leith, W. and W. Alvarez, Structure of the Vakhsh fold-and-thrust belt, Tadjik SSR (Reply), *Bull Geol Soc Am. 97*, 906-908, 1986.

Leith, W. and D. W. Simpson, Seismic domains within the Gissar Kokshal seismic zone, Soviet central Asia, *J. Geophys. Res. 91*, 689-699, 1986.

Lerche, I., ed., *Review of Salt Domes and Salt Tectonics*, Academic, in press, 1986.

Luchinkov, V. S., Upper Jurassic halogen deposits of southeast Central Asia, *Trudy Inst. Geol. i Geofiz 535*, 19-33, 1982.

Racine, D. and P. Klouda, Seismicity of the salt areas of Texas, Louisiana, Oklahoma and Kansas, *Tech Report AL-79-3*, 27 pp., Teledyne Geotech, Alexandria, 1979.

Sadikov, T. S., Halogenic formations of southwest Tadjikistan, in *Structure and Condition of Formation of Salt Formations*, edited by A. L. Yanshin, pp. 137-143, Nauka, Novosibirsk,1981.

Simpson, D. W. and S. K. Negmatullaev, Induced seismicity at Nurek reservoir, Tadjikistan, USSR, *Bull. Seis. Soc. Am. 71*, 1561-1586, 1981.

Simpson, D. W., Triggered earthquakes, *Ann. Rev. Earth Planet. Sci 14*, 21-42, 1986.

Talbot, C. J. and R. J. Jarvis, Age, budget and dynamics of an active salt extrusion in Iran, *J. Struct. Geol 6*, 521-533, 1984.

Zapol'skiy, K. K., and G. M. Loginova, Features of strong, shallow-focused earthquakes in Tadjikistan, *Physics of the Solid Earth 20* (4), p.305-310, 1984.

Zemletryacenniye v SSSR, 1964-1980, Nauka, Moscow.

William Leith and David W. Simpson, Lamont-Doherty Geol. Obs., Palisades, N.Y. 10964.

(Received July 3, 1986
revised August 22, 1986
accepted August 25, 1986)

Potential Uses of the New York State Seismic Array for Teleseismic and Regional Studies

Arthur L. Lerner-Lam
Lamont-Doherty Geological Observatory, Columbia University

1. Introduction

Apart from their utility to the study of regional seismicity, the use of regional seismic networks for the study of the properties of teleseismic travel times and waveforms is well established. Studies of the crust and upper mantle subjacent to array installations have been done at LASA and NORSAR [*e.g. Aki*, 1973; *Aki et al.*, 1977] and SCARLET [*e.g. Humphreys et al.*, 1984]. Arrays have also been useful for the study of distal structure. *Bungum and Capon* [1974] used LASA recordings to measure apparent back azimuths of Rayleigh waves. *Engdahl* [1968] used LASA records to identify and study *PKiKP* and *PmKP* arrivals. *Husebye et al.* [1976] used NORSAR to measure the properties of *PKIKP* precursors, and *Chang and Cleary* [1978, 1981] and *Doornbos* [1980] used arrays to measure the properties of *PKKP*. NORSAR has also been used to study the nature of *P*-diffracted and its decay into the core shadow [*Doornbos and Mondt*, 1979]. The recently operational NARS network [*Dost et al.*, 1984] is being used to assemble a broad range of observations of fundamental and higher-mode surface waveform characteristics and to study the properties of phases converted at upper-mantle discontinuities [*Paulssen*, 1985; *Dost*, 1986]. In this report, we explore the utility of the New York State Seismic Array (NYSSA), operated by Lamont-Doherty, for studies of regional variability of structure and the properties of the core-mantle boundary and D''.

Waveform studies using arrays offer the advantage of signal enhancement by assuming (with some justification) that the background noise is uncorrelated at frequencies of interest. Various stacking and beaming procedures have been designed to optimize the response of the array to the particular signal being evaluated [*e.g. Capon et al.*, 1967; *Nolet and Panza*, 1976; *Husebye et al.*, 1976; *Ingate et al.*, 1985]. Such procedures depend critically upon the physical design of the array, that is, the disposition of the instruments. While these procedures elevate the accuracy of various sorts of signal measurements, of somewhat more importance for global studies is the position of the array relative to seismogenic regions [*Gee et al.*, 1985]. NYSSA is situated ideally with respect to the seismogenic zones of the southwestern Pacific for the study of the core phases belonging to the *PKP* group. In addition to their instrinsic interest, *PKP* phases arrive at the array with nearly vertical incidence, and provide a reasonable input signal with which near-receiver transfer function can be evaluated, and small-scale regional structure can be estimated. Of importance to the accurate interpretation of these arrivals is a measure of the coherence of the signal, and the response of the array to incoming signals of near vertical incidence. In this report, we assess the utility of using NYSSA for the analysis of these phases. Initial estimates of spatial coherence over a restricted

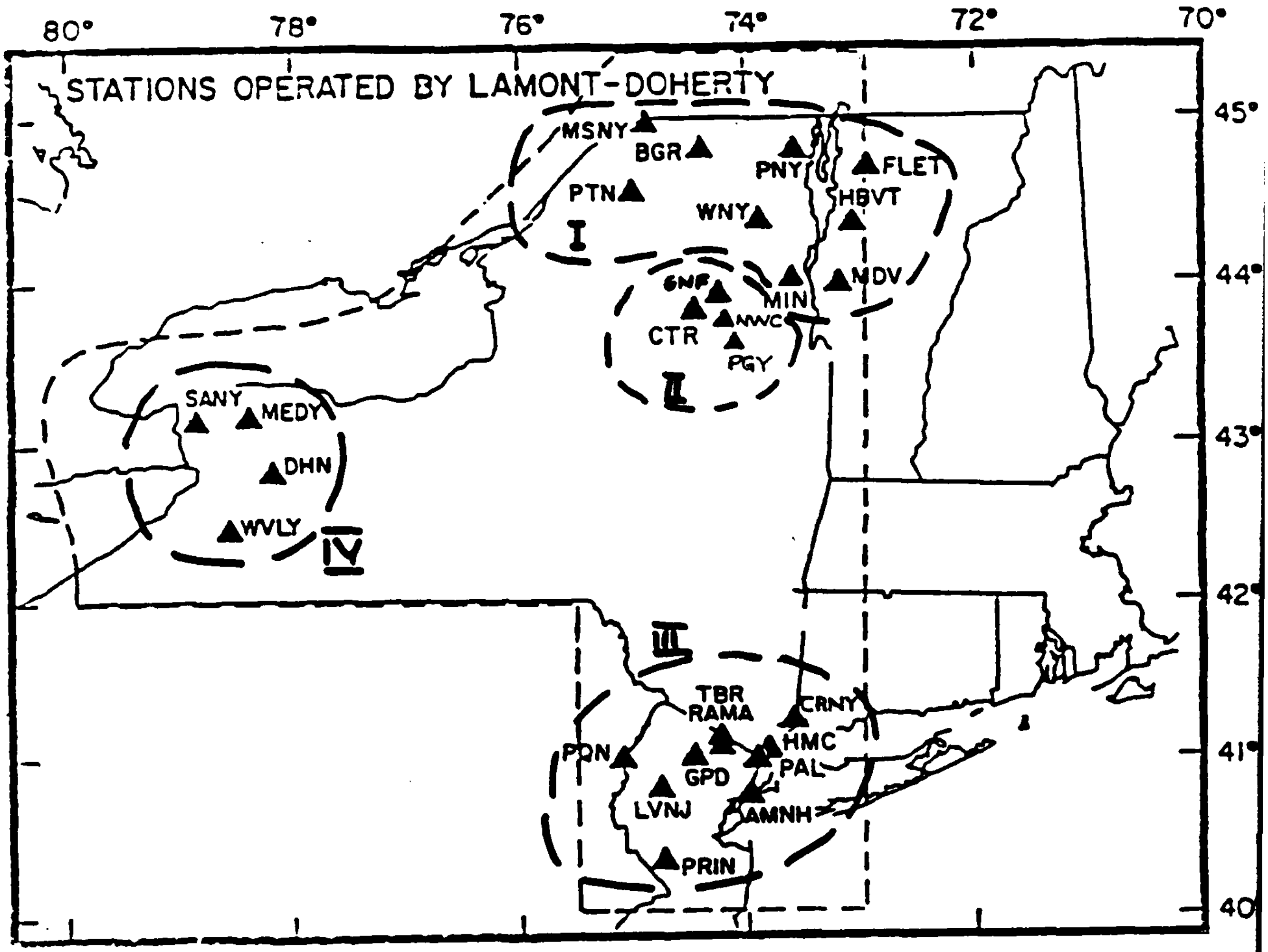

Figure 1: Configuration of New York State Seismic Array as of December 10, 1986. LDGO is located near station PAL in southeastern New York State. Roman numerals refer to subnetworks; each will have a central data recording / transmission site tied to LDGO.

portion of the array will be presented. These measurements are important to a thorough understanding of higher-frequency regional wave propagation, a program of interest to DARPA. Future DARPA-funded research at LDGO will be concerned with the robust estimation of spatial coherence using NYSSA and specially installed sub-arrays, and the implications for crustal and mantle heterogneity beneath the array.

2. Network configuration

The New York State Seismic Array (NYSSA) was developed and installed by Lamont-Doherty Geological Observatory (LDGO) to monitor seismicity in the northeastern United States. The current configuration, shown in Figure 1, comprises 27 stations partitioned into four sub-regional networks in northern New York State, the Adirondacks, southeastern New York and northern New Jersey, and western New York. Station sites were chosen to provide optimal array characteristics for local and regional seismic monitoring experiments. The dotted line surrounds the region in which there is nearly complete detection of events above magnitude 2.0. Sensors have fundamental periods of one or two seconds; together with associated electronics, the total system response is flat to acceleration between .1 and 1 Hz and flat to velocity between 1 and 10 Hz (Figure 2). System output is digitized using a 12-bit A/D with 100 Hz sampling, giving a usable response to 30 Hz. The pre-event memory is variable, and can be adjusted to a maximum of 68 seconds.

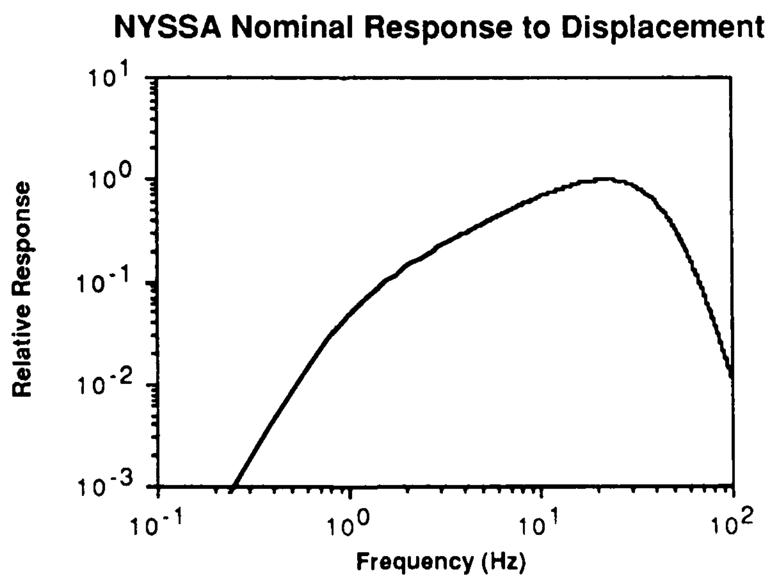

Figure 2: Nominal NYSSA instrument displacement response, after *Lee and Stewart* [1981].

The network operates in triggered mode using a short-term average – long-term average algorithm tuned to seismicity levels in the Northeast. Detected events are transmitted over leased

telephone lines to LDGO using analog telemetry. Although the triggering algorithm is designed to detect local and regional events reliably, teleseismic arrivals, particularly those having higher frequency content, will trigger the network and be recorded. Since the network trigger must be tuned to avoid saturation on small local events, the effective magnitude threshold for teleseisms at core-study distances is greater than about $m_b = 6.0$. Selected analog recordings have been made of events with body-wave magnitudes as low as 5.2 – 5.5, however, with sufficient "eyeball" signal-to-noise levels to be useful for core-phase analysis. To trigger on these events, and to avoid saturation by small local events, the triggering algorithm must be modified to make near real-time estimates of incoming signal azimuth and incidence angle.

3. Comparison of NYSSA and NORSAR for *PKP* analysis

The New York State Seismic Array (NYSSA) was established principally to monitor regional seismicity in the northeastern United States. Teleseismic triggers typically have been used to provide external checks on instrument polarities. NORSAR, on the other hand, was established principally as a network with a well-defined array response to incoming teleseismic arrivals in order to resolve questions associated with nuclear event detection and discrimination, though it has proven very successful in addressing basic earth structure problems [*e.g. Husebye et al.*, 1976; *Aki et al.*, 1977; *Doornbos and Mondt,* 1979].

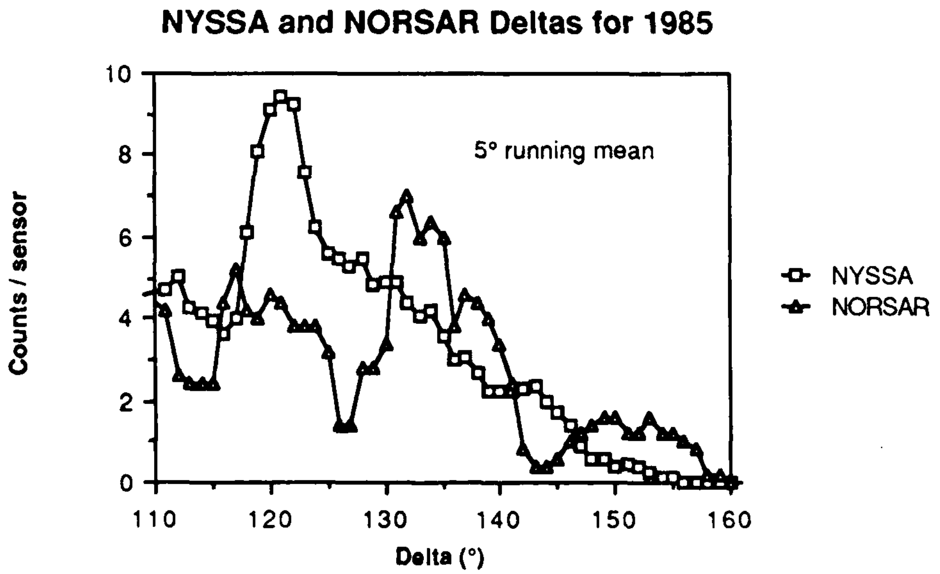

Figure 3: Histogram of expected arrivals per sensor at NYSSA (squares) and NORSAR (triangles) for Pacific Rim earthquakes with $m_b > 5.5$. A 5° running mean has been applied to simulate wider aperture. Seismicity is taken from 1985 PDE catlaogs.

Figure 3 shows a comparison of expected annual arrivals (per sensor) at NYSSA and NORSAR as a function of epicentral distance from Pacific rim events with m_b greater than 5.5, using events in the 1985 PDE catalog. The number of arrivals integrated over the distance range 110° – 160° is about the same for both arrays, but the distributions are different. The NYSSA array has a peak in the arrival histogram between 117° and about 130°, with roughly double the number

of expected arrivals at NORSAR, while NORSAR should see about 50% more arrivals bewteen 130° and 140° than NYSSA. (Indeed, the study of *DF*-precursors by *Husebye et al.* [1976] used events concentrated around 131° and 136°, corresponding roughly to the peaks in the NORSAR histogram in Figure 3.) Overall the NYSSA histogram is smoother, reflecting a more favorable distribution of event geometry and a wider aperture. NORSAR, however, should have greater detection capabilities due to its more controlled array response [*Dahle et al.*, 1975], a factor which we will investigate for NYSSA. The total azimuthal sampling is comparable between the two arrays, though of course, the patches of the core sampled by each array are different. Our point here is not to focus on dissimilar aspects of NYSSA and NORSAR, but merely to demonstrate that both NORSAR and NYSSA are potentially capable of illuminating equivalent portions of P' branches. Examples of *DF*-precursor waveforms from NORSAR are published in *Husebye et al.* [1976]. Examples of waveforms from NYSSA are shown in the next section.

4. Initial observations of *PKP*

We have examined 22 teleseismic triggers from events in the southwest Pacific and Indonesia covering an epicentral range from 111° to 148°. The network triggers on P'_{DF} or P'_{BC} for these events, and there is enough pre-event memory in the standard configuration to obtain good recordings of *DF*-precursors or the $AB - BC - DF$ crossovers. At these azimuths, the network aperture is about 5°. Examples of three record sections exhibiting *DF*-precursors are shown in Figures 4, 5, and 6. Figure 7 shows a record section illuminating the $BC - DF$ crossover.

Event 860115.2017, shown in Figure 4, is one of the closest events for which we have observed unambiguous precursors (119° – 124°). (To our knowledge, these are among the closest observations of *DF*-precursors yet collected.) *DF*-precursors are well-observed on stations beyond 122° (these are Adirondack sites) with impulsive onset and a ringing behavior of nearly constant amplitude up to the *DF* arrival. Total length of the precursive wavetrain is 11 – 12 seconds. Noise levels at the stations vary, and the precursor is not detected easily at BING, WND, or SANY, although there is some indication of anomalous energy preceding *DF* by about 6 – 7 seconds at DHN (119.8°). Figures 5 and 6 display events 840806.1201 and 850111.1441, respectively, each illuminating the same portion of the P' travel-time curve (132° – 137°). Precursive arrivals to *DF* are clear in Figure 5, but the wavetrain is longer (13 – 16 seconds) and more emergent than in Figure 4, with amplitudes increasing toward the *DF* arrival (compare, for example, WPNY in Figures 4 and 5). These events are at two different azimuths, however, and it is not yet certain whether we are observing source effects, source site effects, or differences in the characteristics of D'' or the CMB between the two paths. Observations of short-period P at closer distances can assist in the interpretation of this difference. We note, however, that the onset times are qualitatively consistent with the theoretical least times given in *Haddon and Cleary* [1974, Figure 6]. We contrast 840806.1201 in Figure 5 with 850111.1441 in Figure 6, where precursive arrivals, if present at all, are of much smaller amplitude relative to *DF*. Again, we cannot tell

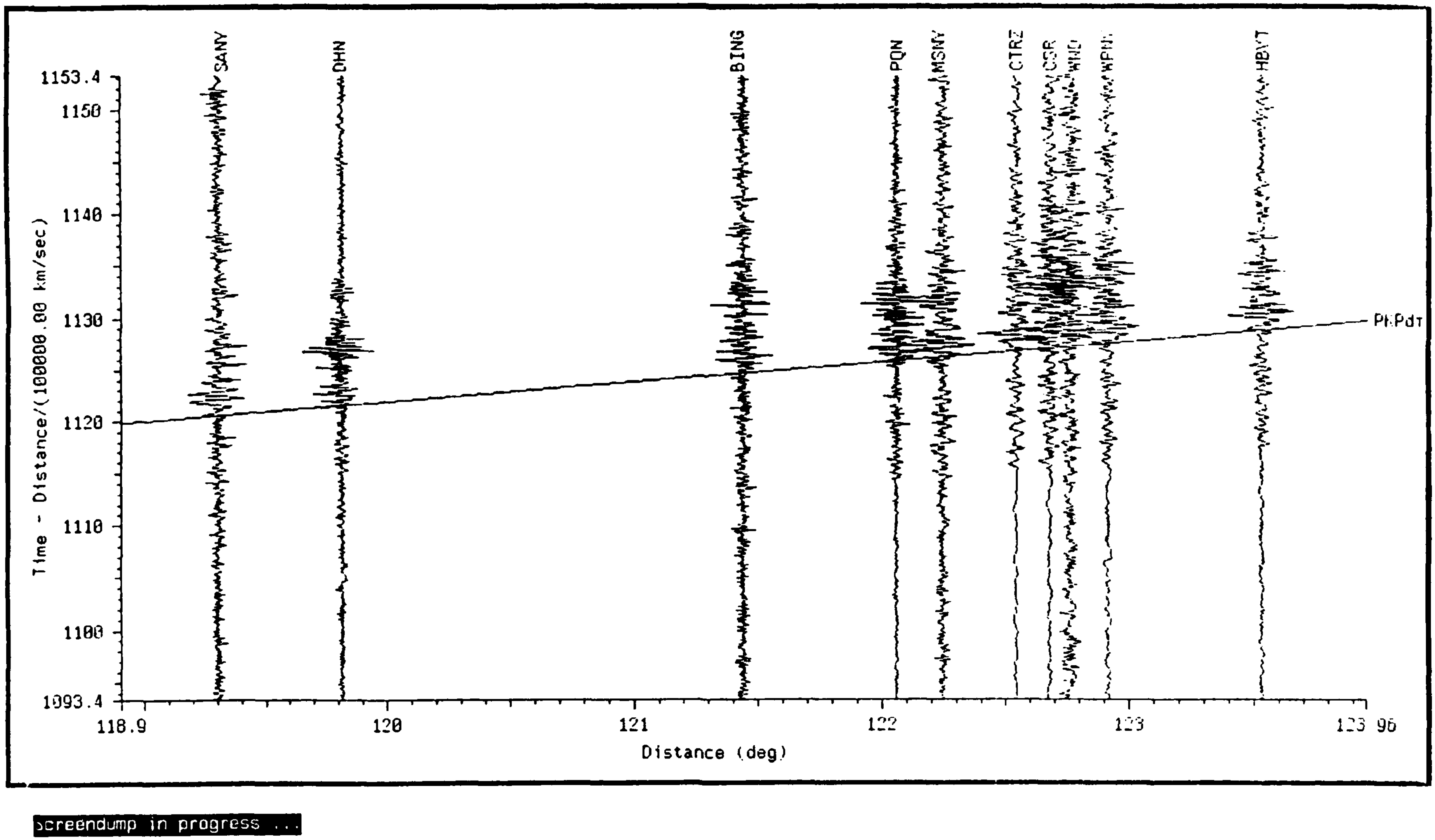

Figure 4: Record section comprising selected recordings on NYSSA of event 860115.2017, h=145 km. *DF*-precursor arrivals are evident as distributed waveforms with impulsive onsets at distances beyond 122°. Travel-time curve is JB with constant offset added to match observed *DF* moveout. One minute of record is shown.

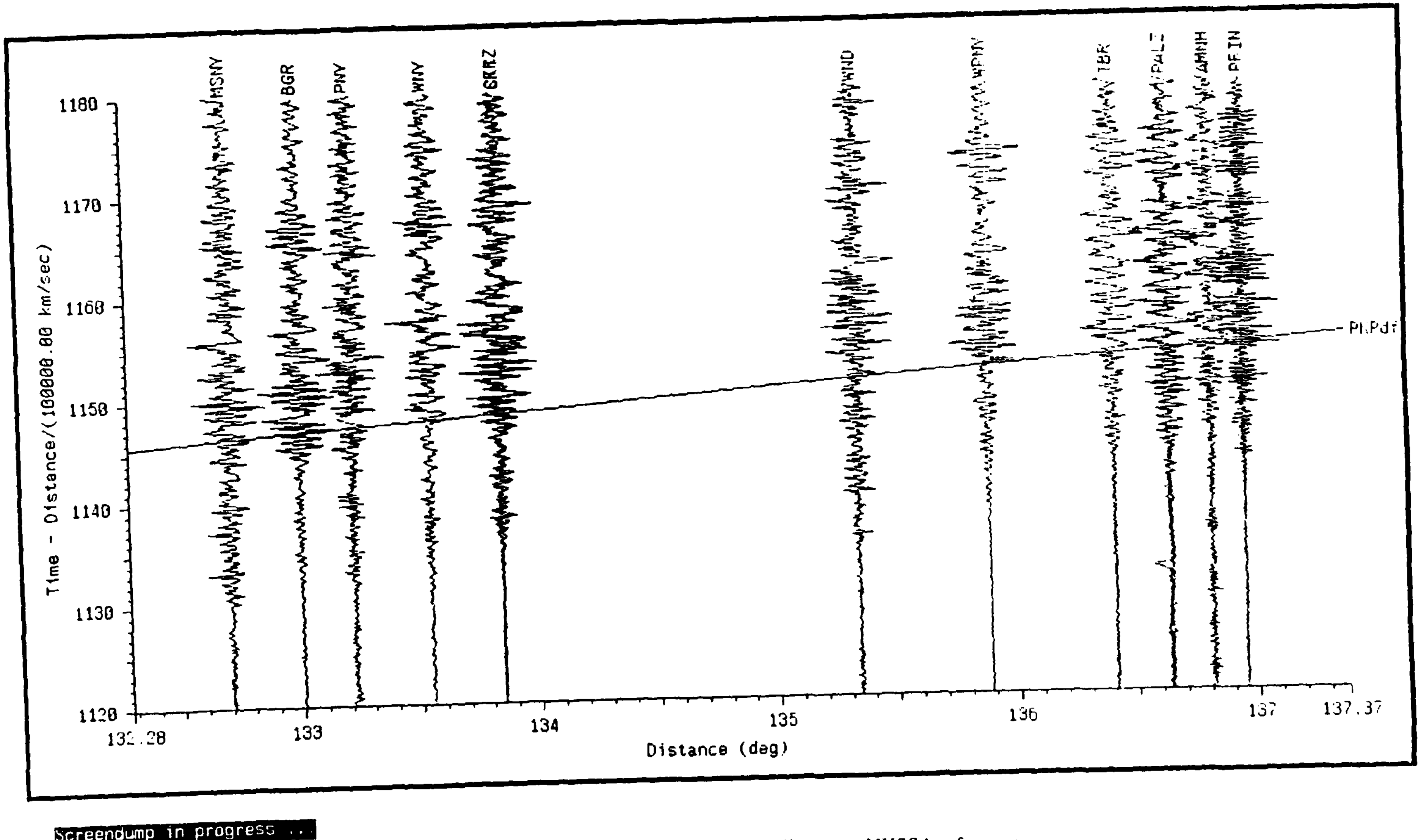

Figure 5: Record section comprising selected recordings on NYSSA of event 840806.1201, h=242 km. Clear precursive arrivals are evident at all distances, although the onset of the precursor is more emergent than observed in Figure 4.

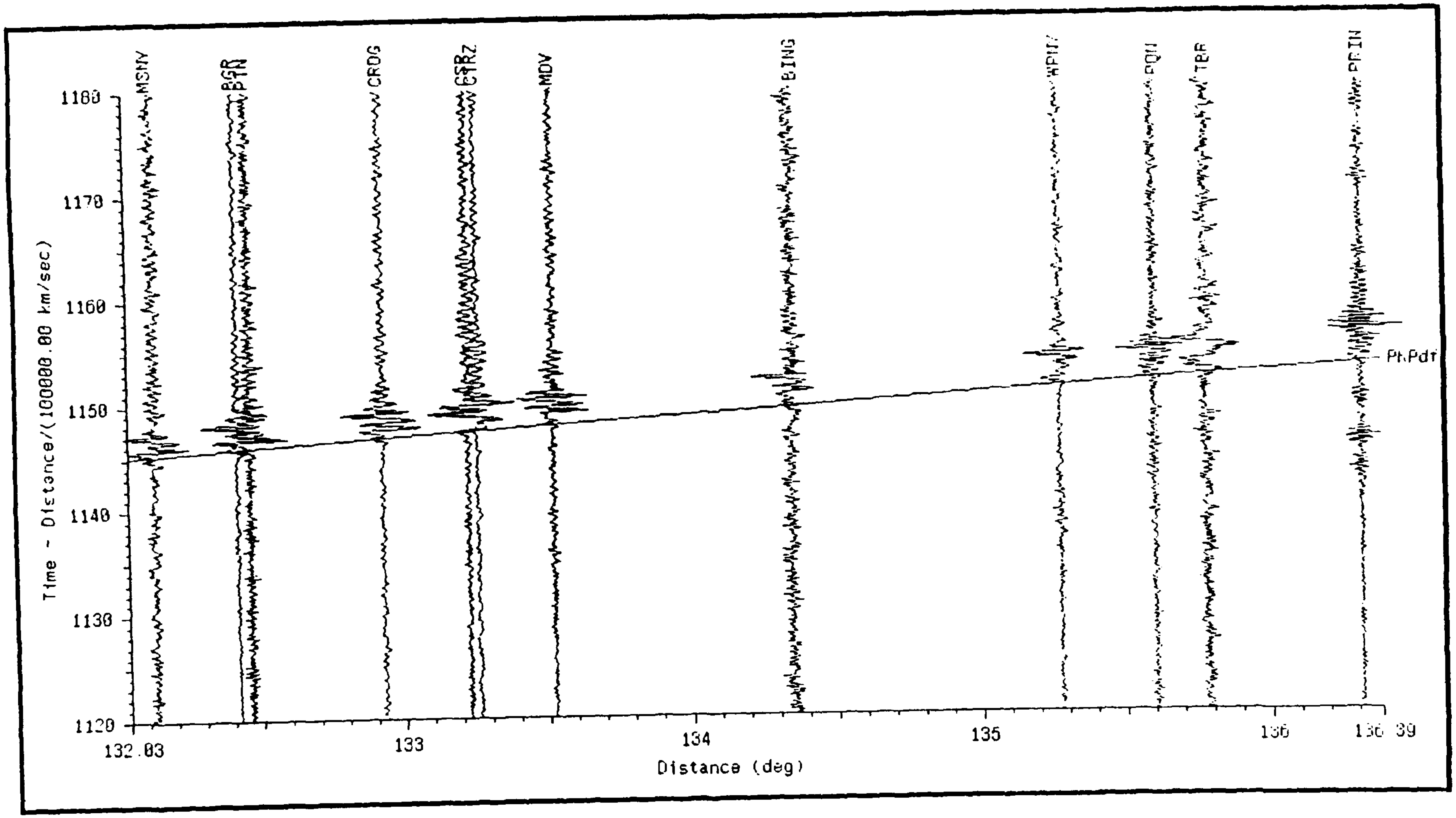

Figure 6: Record section comprising selected recordings on NYSSA of event 850111.1441, h=189 km. Though having nearly the same range and back azimuth as the record section shown in Figure 5, the DF-precursors shown here are much less evident. Note also that the P' arrival is much simpler.

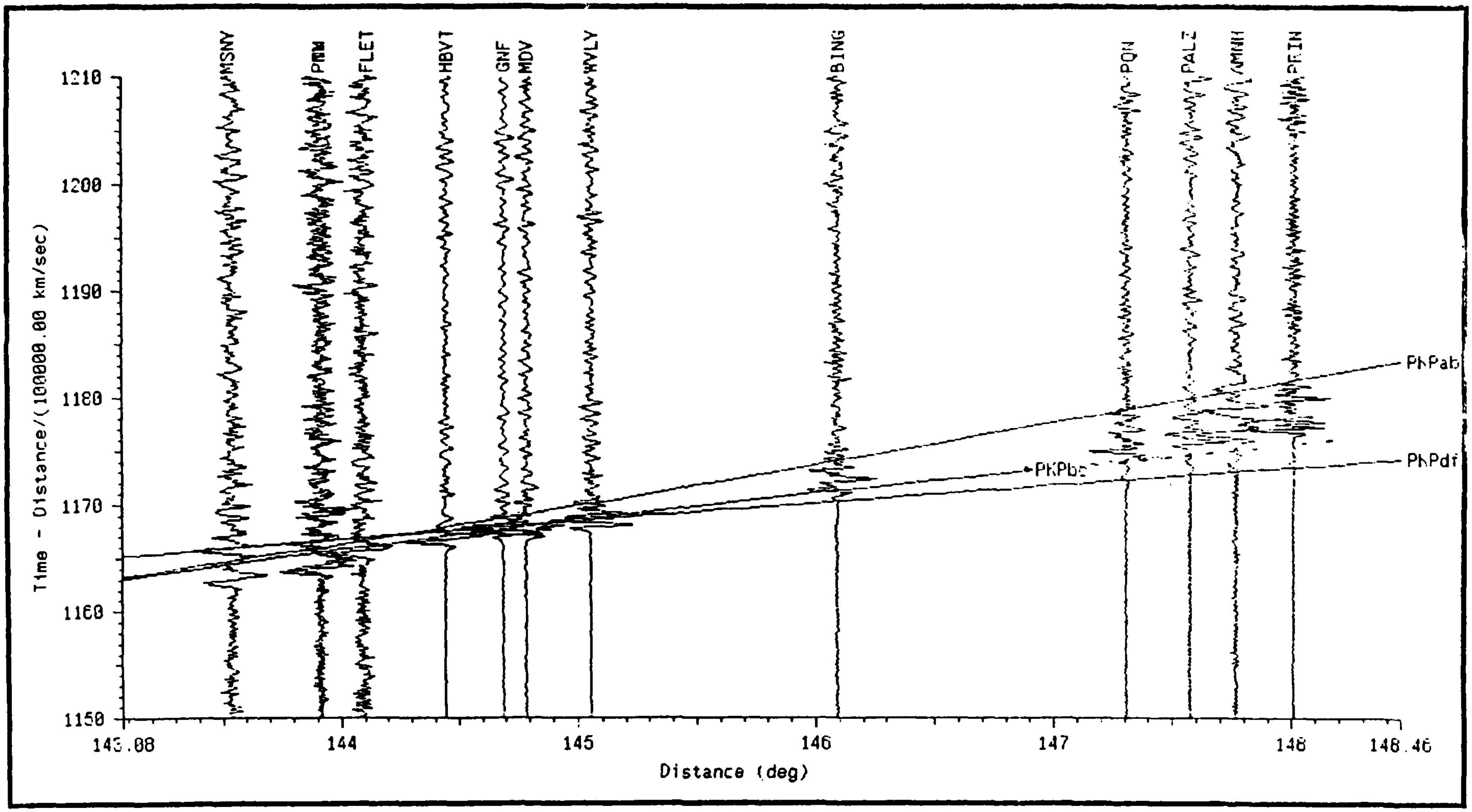

Screendump in progress ..

Figure 7: Record section comprising selected recordings on NYSSA of event 850413.0106, h=99 km. The large amplitude arrival is P'_{BC}; *DF* appears as the much smaller arrival beyond 147°. Travel-time curves are JB, with a constant offset added to match the *DF* branch.

without further study whether we are observing the effects of source complexity or CMB heterogeneity (the *DF* wavefoms in Figure 6 are much simpler than those in Figure 5).

Figure 7 displays a record section collected just beyond the *B*-cusp at about 143°. The dominant arrival is P'_{BC}, with P'_{DF} appearing only as a small, low-amplitude arrival beyond 145°. The travel-time curves shown are calculated for the JB model, with a constant time offset of 2.1 s added in order to line up P'_{DF} with the data. The P'_{DF} and P'_{BC} travel times appear to be well fit by the offset model at distances greater than 146°, but for distances closer than the *BC* – *DF* crossover, the P'_{BC} arrivals are much earlier (about 2 seconds) than predicted.

Figures 4 – 7 are given as examples of the data quality and the detail available when station sites are densely distributed at appropriate epicentral distances. A more comprehensive analysis of these data is underway at LDGO, and will be the subject of another publication.

In the discussion that follows, we use the PKP_{DF} waveform from event 840806.1201 to estimate signal coherences.

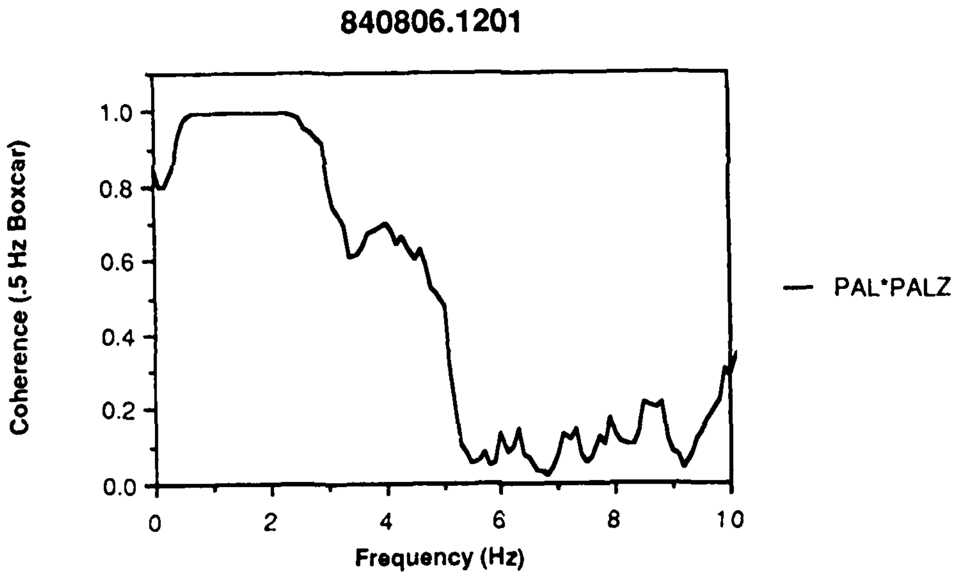

Figure 8: Amplitude coherence between two different sensors situated on the same pier, for one-minute signal duration, using the *PKP-DF* trigger for event 840806.1201. Cross-spectrum and auto-spectra estimates are smoothed with a .5 Hz frequency boxcar. Coherence is high out to 3 Hz, and acceptable to 5 Hz. Lower values of coherence at low frequencies are due to instrumental drift.

5. Coherence estimates

For a period of time, LDGO operated two sensors (Geospace HS-10 and a Ranger, both with natural periods of 1 s) on the same pier at PAL, using amplifiers and filters having characteristics identical to the rest of the network. Figure 8 shows their normalized coherence

(smoothed over .5 Hz spectral window) from DC to 10 Hz for the PKP_{DF} signal produced by 840806.1201. The coherence is near unity between .5 and 2.5 Hz, and maintains a level of about .6 to 5 Hz. There is some incoherency below .5 Hz which is noticeable in the time series as long-period drift. This is easy to spot upon examination, however, and is not a factor in our interpretation of the waveforms. Evidently, there are no pathologic instabilities in the electronics which might impact signal coherence below 2 Hz. In what follows, we use 2 Hz as the upper frequency limit for our analysis.

We concentrate in this report on coherence measurements at the Adirondack and northern New York sites (sub-nets I and II in Figure 1), using six vertical-component stations at CTR, MSNY, BGR, WNY, PNY, and SKT (near GNF). For the most part, the stations are situated on hard-rock with some glacial till cover with low cultural and microseismic noise characteristics [LDGO field reports]. Inter-station spacing ranges from 24.7 km to 128.8 km, and the median spacing is 97.7 km. For these preliminary studies, we extracted one minute of *PKP* signal beginning with the *DF*-precursor and tapered the time series with a 10% cosine. We assume that the instrument responses are characterized by the nominal poles and zeros given in *Lee and Stewart* [1981].

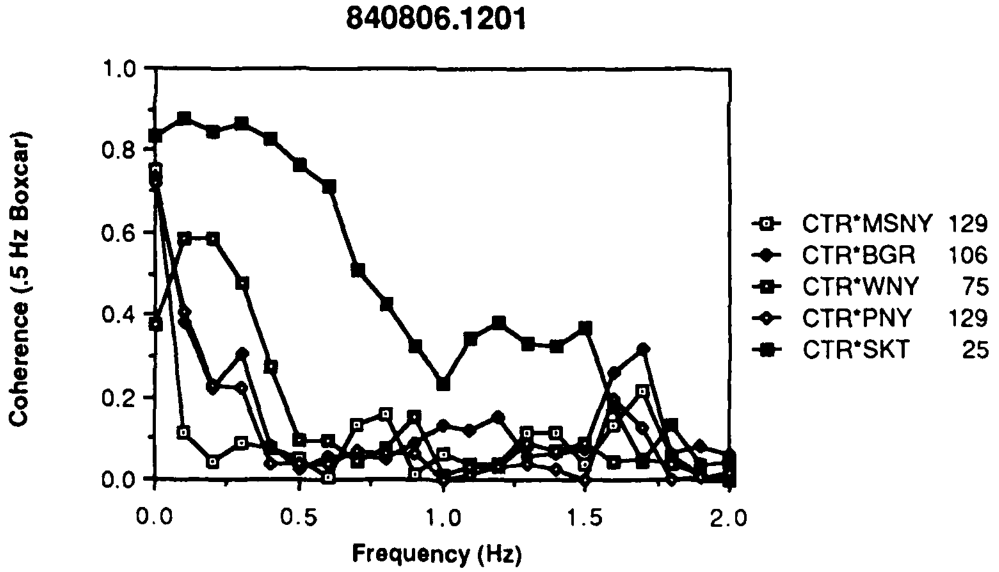

Figure 9: Inter-station coherence as a function of frequency between CTR and other stations of the Adirondack and northern New York subnets, for one-minute signal duration. Numbers to the right of the legend give inter-station spacing in kilometers. Coherence levels are lower for increased station separation as expected.

Figure 9 shows coherence estimates (.5 Hz spectral window smoothing) between CTR and the other five stations as a function of frequency. The best coherence is exhibited for CTR*SKT, which also have the closest inter-station spacing (between 2 and 3 signal wavelengths). Even so, the coherence drops below .5 above .75 Hz. Not surprisingly, sub-array heterogeneity affects the

coherence estimate. Figure 10 displays coherence for two station pairs having nearly identical inter-station spacing (WNY*PNY and WNY*SKT). Differences in the coherence curves are indicators of differences in station response or station site effects (noise, transmission losses, differences in structure, and so on). The curves have similar fall-offs above about .7 Hz, though the WNY*SKT coherence is lower.

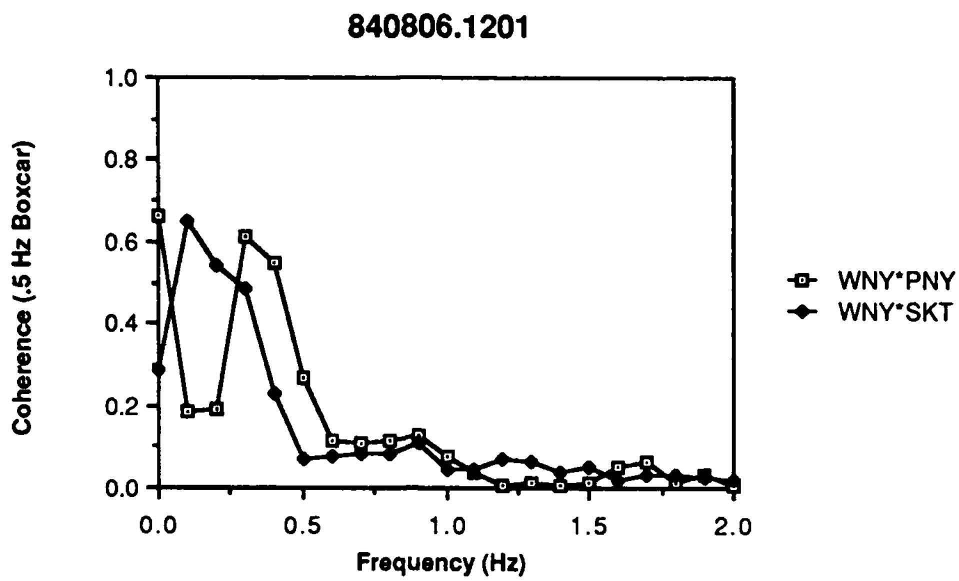

Figure 10: Coherence between WNY, PNY, and SKT. WNY is 54 km from both PNY and SKT. PNY is 109 km from SKT. Differences in coherence indicate that the distribution of heterogeneities is not isotropic.

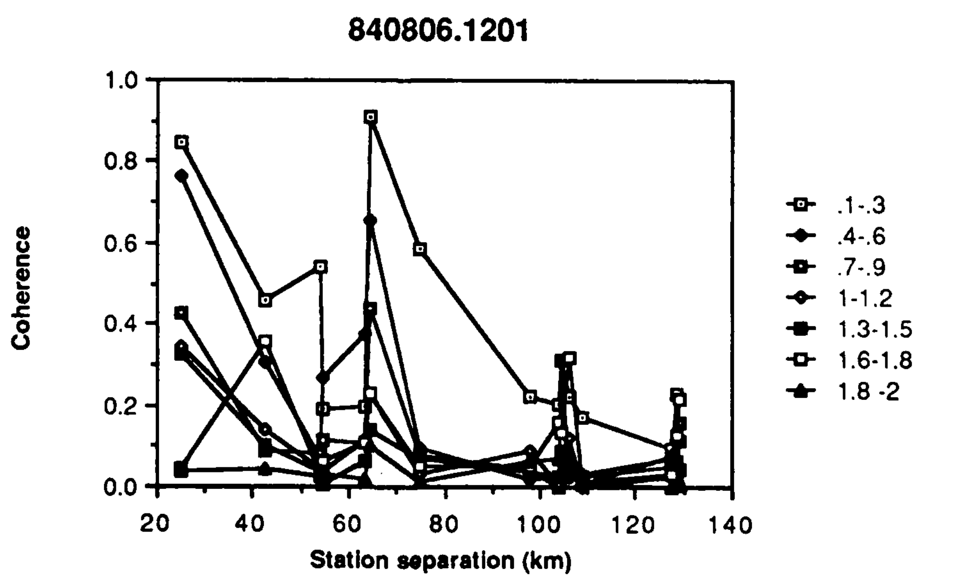

Figure 11: Coherence as a function of inter-station spacing for each of several narrow bands. The "hole" between 50 and 60 km is probably due to improper instrument response.

Figure 11 displays coherence as a function of inter-station spacing for several narrow bands

in frequency. The coherence "hole" between 50 and 60 km is presumably due to problems with the station at WNY (1-second vs. 2-second seismometer, site characteristics), though nothing in the field installation notes indicates any special siting problems or instrumental defects. Relatively high coherence is seen at low-frequencies (<.5 Hz) out to distances of about 60 to 80 km (3-5 crustal wavelengths), somewhat greater than observed at LASA [*Aki*, 1973] or NORSAR [*Bungum et al.*, 1971].

While these results are very preliminary (and point to the necessity of obtaining appropriate instrument response functions), they nevertheless show the potential usefulness of a well-situated array for teleseismic structural studies and subjacent site structure.

6. Plans for further analysis

Future work will include the reconstruction of individual station calibration responses (particularly phase responses) from field installation and maintenance notes. We will also develop more robust coherence estimation techniques, and include more events in our coherence estimates. The one-minute time windows used in our estimation include not only primary signal but some clearly reverberatory waveforms; future analyses will examine shorter time windows and will use polarization analysis to detect mode conversions. In addition, LDGO is installing new permanent instrumentation and acquiring new portable instruments. These will be deployed in various configurations for both intra-network coherence and *PKP* studies.

7. References

Aki, K., Scattering of *P* waves under the Montana LASA, *J. Geophys. Res.*, **78**, 1334-1346, 1973.

Aki, K., A. Christoffersson, and E.S. Husebye, Determination of the three-dimensional structure of the lithosphere, *J. Geophys. Res.*, **82**, 277-296, 1977.

Bungum, H., and J. Capon, Coda pattern and multipath propagation of Rayleigh waves at NORSAR, *Phys. Earth Planet. Int.*, **9**, 111-127, 1974.

Bungum, H., E.S. Husebye, and F. Ringdal, The NORSAR array and preliminary results of data analysis, *Geophys. J. R. Astr. Soc.*, **25**, 115-126, 1971.

Capon, J., R.J. Greenfield, and R.J. Kolker, Multidimensional maximum likelihood processing of a large aperture array, *Proc. IEEE*, **55**, 192-211, 1967.

Chang, A.C., and J.R. Cleary, Precursors to *PKKP*, *Bull. Seism. Soc. Am.*, **68**, 1059-1079, 1978.

Chang, A.C., and J.R. Cleary, Scattered *PKKP*: further evidence for scattering at a rough core-mantle boundary, *Phys. Earth Planet. Int.*, **24**, 15-29, 1981.

Dahle, A., E.S. Husebye, K.A. Berteussen, and A. Christoffersson, Wave scattering effects and seismic velocity measurements, in *Exploitation of Seismograph Networks*, 559-576, Noordhoff, Leoden, Netherlands, 1975.

Doornbos, D.J., The effect of a rough core-mantle boundary on *PKKP*, *Phys. Earth Planet. Int.*, **21**, 351-358, 1980.

Doornbos, D.J., and J.C. Mondt, *P* and *S* waves diffracted around the core and the velocity structure at the base of the mantle, *Geophys. J. R. Astr. Soc.*, **57**, 381-395, 1979.

Dost, B., Preliminary results from higher-mode surface wave measurements in western Europe using the NARS array, *Tectonophysics*, **128**, 289-301, 1986.

Dost, B., A. van Wettum, and G. Nolet, The NARS Array, *Geol. Mijnbouw*, **63**, 381-386, 1984.

Engdahl, E.R., Core phases and the earth's core, Ph.D. thesis, St. Louis University, St. Louis, Mo., 1968.

Gee, L.S., A.L. Lerner-Lam, and T.H. Jordan, Resolving power of higher-mode waveform inversion for Eurasian upper-mantle structure, Semiannual report, Defense Advanced Research Projects Agency, 1985.

Haddon, R.A.W., and J.R. Cleary, Evidence for scattering of seismic *PKP* waves near the mantle-core boundary, *Phys. Earth Planet. Int.*, **8**, 211-234, 1974.

Humphreys, E., R.W. Clayton, and B.H. Hager, A tomographic image of mantle structure beneath southern California, *Geophys. Res. Lett.*, **11**, 625-627, 1984.

Husebye, E.S., D.W. King, and R.A.W. Haddon, Precursors to *PKIKP* and seismic wave scattering near the core-mantle boundary, *J. Geophys. Res.*, **81**, 1870-1882, 1976.

Ingate, S.F., E.S. Husebye, and A. Christoffersson, Regional arrays and optimum data processing schemes, *Bull. Seism. Soc. Am.*, **75**, 1155-1177, 1985.

Lee, W.H.K., and S.W. Stewart, Principles and applications of micorearthquake networks, in, Advances in Geophysics, ed. B. Saltzman, Academic Press, 1981.

Paulssen, H., Upper mantle converted waves beneath the NARS array, *Geophys. Res. Lett.*, **12**, 709-712, 1985.

Nolet, G., and J. Panza, Array analysis of seismic surface waves: limits and possibilities, *Pageoph.*, **114**, 775-790, 1976.

DISTRIBUTION LIST

Dr. Monem Abdel-Gawad
Rockwell International Science Center
1049 Camino Dos Rios
Thousand Oaks, CA 91360

Professor Keiiti Aki
Center for Earth Sciences
University of Southern California
University Park
Los Angeles, CA 90089-0741

Professor Shelton S. Alexander
Geosciences Department
403 Deike Building
The Pennsylvania State University
University Park, PA 16802

Professor Charles B. Archambeau
Cooperative Institute for Research in
Environmental Sciences
University of Colorado
Boulder, CO 80309

Dr. Thomas C. Bache Jr.
Science Applications Int'l Corp.
10210 Campus Point Drive
San Diego, CA 92121

Dr. James Bulau
Rockwell International Science Center
1049 Camino Dos Rios
P.O. Box 1085
Thousand Oaks, CA 91360

Dr. Douglas R. Baumgardt
Signal Analysis and Systems Division
ENSCO, Inc.
5400 Port Royal Road
Springfield, VA 22151-2388

Dr. S. Bratt
Science Applications Int'l Corp.
10210 Campus Point Drive
San Diego, CA 92121

Professor John Ebel
Department of Geology & Geophysics
Boston College
Chestnut Hill, MA 02167

Woodward-Clyde Consultants
Attn: Dr. Lawrence J. Burdick
Dr. Jeff Barker
P.O. Box 93245
Pasadena, CA 91109-3245 (2 copies)

Dr. Roy Burger
1221 Serry Rd.
Schenectady, NY 12309

Professor Robert W. Clayton
Seismological Laboratory
Division of Geological and Planetary
Sciences
California Institute of Technology
Pasadena, CA 91125

Dr. Vernon F. Cormier
Earth Resources Laboratory
Department of Earth, Atmospheric and
Planetary Sciences
Massachusetts Institute of Technology
42 Carleton Street
Cambridge, MA 02142

Professor Anton M. Dainty
Earth Resources Laboratory
Department of Earth, Atmospheric and
Planetary Sciences
Massachusetts Institute of Technology
42 Carleton Street
Cambridge, MA 02142

Dr. Zoltan A. Der
Teledyne Geotech
314 Montgomery Street
Alexandria, VA 22314

Prof. Adam Dziewonski
Hoffman Laboratory
Harvard University
20 Oxford St.
Cambridge, MA 02138

Professor John Ferguson
Center for Lithospheric Studies
The University of Texas at Dallas
P.O. Box 830688
Richardson, TX 75083-0688

Dr. Jeffrey W. Given
Sierra Geophysics
11255 Kirkland Way
Kirkland, WA 98033

Prof. Roy Greenfield
Geosciences Department
403 Deike Building
The Pennsylvania State University
University Park, PA 16802

Professor David G. Harkrider
Seismological Laboratory
Division of Geological and Planetary Sciences
California Institute of Technology
Pasadena, CA 91125

Professor Donald V. Helmberger
Seismological Laboratory
Division of Geological and Planetary Sciences
California Institute of Technology
Pasadena, CA 91125

Professor Eugene Herrin
Institute for the Study of Earth & Man
Geophysical Laboratory
Southern Methodist University
Dallas, TX 75275

Professor Robert B. Herrmann
Department of Earth and Atmospheric Sciences
Saint Louis University
Saint Louis, MO 63156

Professor Lane R. Johnson
Seismographic Station
University of California
Berkeley, CA 94720

Professor Thomas H. Jordan
Department of Earth, Atmospheric and Planetary Sciences
Massachusetts Institute of Technology
Cambridge, MA 02139

Dr. Alan Kafka
Department of Geology & Geophysics
Boston College
Chestnut Hill, MA 02167

Professor Charles A. Langston
Geosciences Department
403 Deike Building
The Pennsylvania State University
University Park, PA 16802

Professor Thorne Lay
Department of Geological Sciences
1006 C.C. Little Building
University of Michigan
Ann Arbor, MI 48109-1063

Dr. George R. Mellman
Sierra Geophysics
11255 Kirkland Way
Kirkland, WA 98033

Professor Brian J. Mitchell
Department of Earth and Atmospheric Sciences
Saint Louis University
Saint Louis, MO 63156

Professor Thomas V. McEvilly
Seismographic Station
University of California
Berkeley, CA 94720

Dr. Keith L. McLaughlin
Teledyne Geotech
314 Montgomery Street
Alexandria, VA 22314

Professor Otto W. Nuttli
Department of Earth and Atmospheric Sciences
Saint Louis University
Saint Louis, MO 63156

Professor Paul G. Richards
Lamont-Doherty Geological Observatory of Columbia University
Palisades, NY 10964

Dr. Norton Rimer
S-Cubed
A Division of Maxwell Laboratory
P.O. 1620
La Jolla, CA 92038-1620

Professor Larry J. Ruff
Department of Geological Sciences
1006 C.C. Little Building
University of Michigan
Ann Arbor, MI 48109-1063

Professor Charles G. Sammis
Center for Earth Sciences
University of Southern California
University Park
Los Angeles, CA 90089-0741

Dr. David G. Simpson
Lamont-Doherty Geological Observatory
of Columbia University
Palisades, NY 10964

Dr. Jeffrey L. Stevens
S-CUBED,
A Division of Maxwell Laboratory
P.O. Box 1620
La Jolla, CA 92038-1620

Professor Brian Stump
Institute for the Study of Earth
and Man
Geophysical Laboratory
Southern Methodist University
Dallas, TX 75275

Professor Ta-liang Teng
Center for Earth Sciences
University of Southern California
University Park
Los Angeles, CA 90089-0741

Dr. R. B. Tittmann
Rockwell International Science Center
1049 Camino Dos Rios
P.O. Box 1085
Thousand Oaks, CA 91360

Professor M. Nafi Toksoz
Earth Resources Laboratory
Department of Earth, Atmospheric and
Planetary Sciences
Massachusetts Institute of Technology
42 Carleton Street
Cambridge, MA 02142

Professor Terry C. Wallace
Department of Geosciences
Building #11
University of Arizona
Tucson, AZ 85721

Prof. John H. Woodhouse
Hoffman Laboratory
Harvard University
20 Oxford St.
Cambridge, MA 02138

Dr. G. Blake
US Dept.of Energy/DP 331
Forrestal Building
1000 Independence Ave.
Washington, D.C. 20585

Dr. Michel Bouchon
Universite Scientifique et
Medicale de Grenoble
Laboratoire de Geophysique
Interne et Tectonophysique
I.R.I.G.M.-B.P. 68
38402 St. Martin D'Heres
Cedex FRANCE

Dr. Hilmar Bungum
NTNF/NORSAR
P.O. Box 51
Norwegian Council of Science,
Industry and Research, NORSAR
N-2007 Kjeller, NORWAY

Dr. Alan Douglas
Ministry of Defense
Blacknest, Brimpton, Reading RG7-4RS
UNITED KINGDOM

Professor Peter Harjes
Institute for Geophysik
Rhur University
Bochum
P.O. Box 102148
4630 Bochum 1
FEDERAL REPUBLIC OF GERMANY

Dr. James Hannon
Lawrence Livermore National Laboratory
P.O. Box 808
Livermore, CA 94550

Dr. E. Husebye
NTNF/NORSAR
P.O. Box 51
N-2007 Kjeller, NORWAY

Dr. Arthur Lerner-Lam
Lamont-Doherty Geological Observatory
of Columbia University
Palisades, NY 10964

Mr. Peter Marshall
Procurement Executive
Ministry of Defense
Blacknest, Brimpton, Reading RG7-4RS
UNITED KINGDOM

Dr. B. Massinon
Societe Radiomana
27, Rue Claude Bernard
75005, Paris, FRANCE

Dr. Pierre Mechler
Societe Radiomana
27, Rue Claude Bernard
75005, Paris, FRANCE

Mr. Jack Murphy
S-CUBED
Reston Geophysics Office
11800 Sunrise Valley Drive
Suite 1212
Reston, VA 22091

Dr. Svein Mykkeltveit
NTNF/NORSAR
P.O. Box 51
N-2007 Kjeller, NORWAY

Dr. Carl Newton
Los Alamos National Laboratory
P.O. Box 1663
Mail Stop C 335, Group ESS3
Los Alamos, NM 87545

Dr. Peter Basham
Earth Physics Branch
Department of Energy and Mines
1 Observatory Crescent
Ottawa, Ontario
CANADA K1A OY3

Professor J. A. Orcutt
Geological Sciences Division
Univ. of California at San Diego
La Jolla, CA 92093

Dr. Frank F. Pilotte
Director of Geophysics
Headquarters Air Force Technical
Applications Center
Patrick AFB, Florida 32925-6001

Professor Keith Priestley
University of Nevada
Mackay School of Mines
Reno, Nevada 89557

Mr. Jack Raclin
USGS - Geology, Rm 3C136
Mail Stop 928 National Center
Reston, VA 22092

Dr. Frode Ringdal
NTNF/NORSAR
P.O. Box 51
N-2007 Kjeller, NORWAY

Dr. George H. Rothe
Chief, Research Division
Geophysics Directorate
Headquarters Air Force Technical
Applications Center
Patrick AFB, Florida 32925-6001

Dr. Alan S. Ryall, Jr.
Center for Seismic Studies
1300 North 17th Street
Suite 1450
Arlington, VA 22209-2308

Dr. Jeffrey L. Stevens
S-CUBED,
A Division of Maxwell Laboratory
P.O. Box 1620
La Jolla, CA 92038-1620

Dr. Lawrence Turnbull
OSWR/NED
Central Intelligence Agency
CIA, Room 5G48
Washington, DC 20505

Professor Steven Grand
Department of Geology
245 Natural History Bldg
1301 West Green Street
Urbana, IL 61801

DARPA/PM
1400 Wilson Boulevard
Arlington, VA 22209

Defense Technical Information Center
Cameron Station
Alexandria, VA 22314 (12 copies)

Defense Intelligence Agency
Directorate for Scientific and
Technical Intelligence
Washington, D.C. 20301

Defense Nuclear Agency
Shock Physics Directorate/SS
Washington, D.C. 20305

Defense Nuclear Agency/SPSS
ATTN: Dr. Michael Shore
6801 Telegraph Road
Alexandria, VA 22310

AFOSR/NPG
ATTN: Director
Bldg 410, Room C222
Bolling AFB, Washington, D.C. 20332

AFTAC/CA (STINFO)
Patrick AFB, FL 32925-6001

AFWL/NTESC
Kirtland AFB, NM 87171

U.S. Arms Control & Disarmament Agency
ATTN: Mrs. M. Hoinkes
Div. of Multilateral Affairs, Rm 5499
Washington, D.C. 20451

U.S. Geological Survey
ATTN: Dr. T. Hanks
National Earthquake Research Center
345 Middlefield Road
Menlo Park, CA 94025

SRI International
333 Ravenswood Avenue
Menlo Park, CA 94025

Center for Seismic Studies
ATTN: Dr. C. Romney
1300 North 17th Street
Suite 1450
Arlington, VA 22209 (3 copies)

Dr. Robert Blandford
DARPA/GSD
1400 Wilson Boulevard
Arlington, VA 22209-2308

Ms. Ann Kerr
DARPA/GSD
1400 Wilson Boulevard
Arlington, VA 22209-2308

Dr. Ralph Alewine III
DARPA/GSD
1400 Wilson Boulevard
Arlington, VA 22209-2308

Mr. Edward Giller
Pacific Sierra Research Corp.
1401 Wilson Boulevard
Arlington, VA 22209

Science Horizons, Inc.
Attn: Dr. Bernard Minster
Dr. Theodore Cherry
710 Encinitas Blvd., Suite 101
Encinitas, CA 92024 (2 copies)

Dr. Jack Evernden
USGS - Earthquake Studies
345 Middlefield Road
Menlo Park, CA 94025

Dr. Lawrence Braile
Department of Geosciences
Purdue University
West Lafayette, IN 47907

Dr. G.A. Bollinger
Department of Geological Sciences
Virginia Polytechnical Institute
21044 Derring Hall
Blacksburg, VA 24061

Dr. L. Sykes
Lamont Doherty Geological Observatory
Columbia University
Palisades, NY 10964

Dr. S.W. Smith
Geophysics Program
University of Washington
Seattle, WA 98195

Dr. L. Timothy Long
School of Geophysical Sciences
Georgia Institute of Technology
Atlanta, GA 30332

Dr. N. Biswas
Geophysical Institute
University of Alaska
Fairbanks, AK 99701

Dr. Freeman Gilbert
Institute of Geophysics & Planetary Physics
Univ. of California at San Diego
P.O. Box 109
La Jolla, CA 92037

Dr. Pradeep Talwani
Department of Geological Sciences
University of South Carolina
Columbia, SC 29208

University of Hawaii
Institute of Geophysics
Attn: Dr. Daniel Walker
Honolulu, HI 96822

Dr. Donald Forsyth
Department of Geological Sciences
Brown University
Providence, RI 02912

Dr. Jack Oliver
Department of Geology
Cornell University
Ithaca, NY 14850

Dr. Muawia Barazangi
Geological Sciences
Cornell University
Ithaca, NY 14853

Rondout Associates
Attn: Dr. George Sutton
Dr. Jerry Carter
Dr. Paul Pomeroy
P.O. Box 224
Stone Ridge, NY 12484 (3 copies)

Dr. M. Sorrells
Geotech/Teledyne
P.O. Box 28277
Dallas, TX 75228

Dr. Bob Smith
Department of Geophysics
University of Utah
1400 East 2nd South
Salt Lake City, UT 84112

Dr. Anthony Gangi
Texas A&M University
Department of Geophysics
College Station, TX 77843

Dr. Gregory B. Young
ENSCO, Inc.
5400 Port Royal Road
Springfield, CA 22151

Dr. Ben Menaheim
Weizman Institute of Science
Rehovot, ISRAEL 951729

Weidlinger Associates
Attn: Dr. Gregory Wojcik
620 Hansen Way, Suite 100
Palo Alto, CA 94304

Dr. Leon Knopoff
University of California
Institute of Geophysics & Planetary Physics
Los Angeles, CA 90024

Dr. Kenneth H. Olsen
Los Alamos Scientific Laboratory
Post Office Box 1663
Los Alamos, NM 87545

Prof. Jon F. Claerbout
Prof. Amos Nur
Dept. of Geophysics
Stanford University
Stanford, CA 94305 (2 copies)

Dr. Robert Burridge
Schlumberger-Doll Research Ctr.
Old Quarry Road
Ridgefield, CT 06877

Dr. Eduard Berg
Institute of Geophysics
University of Hawaii
Honolulu, HI 96822

Dr. Robert Phinney
Dr. F.A. Dahlen
Dept. of Geological & Geophysical Sci.
Princeton University
Princeton, NJ 08540 (2 copies)

Dr. Kin-Yip Chun
Geophysics Division
Physics Department
University of Toronto
Ontario, CANADA M5S 1A7

New England Research, Inc.
Attn: Dr. Randolph Martin III
P.O. Box 857
Norwich, VT 05055

Sandia National Laboratory
Attn: Dr. H.B. Durham
Albuquerque, NM 87185

Dr. Gary McCartor
Mission Research Corp.
735 State Street
P. O. Drawer 719
Santa Barbara, CA 93102

Dr. W. H. K. Lee
USGS
Office of Earthquakes, Volcanoes,
& Engineering
Branch of Seismology
345 Middlefield Rd
Menlo Park, CA 94025

AFGL/XO
Hanscom AFB, MA 01731-5000

AFGL/LW
Hanscom AFB, MA 01731-5000

AFGL/SULL
Research Library
Hanscom AFB, MA 01731-5000 (2 copies)

Secretary of the Air Force (SAFRD)
Washington, DC 20330

Office of the Secretary Defense
DDR & E
Washington, DC 20330

HQ DNA
Attn: Technical Library
Washington, DC 20305

Director, Technical Information
DARPA
1400 Wilson Blvd.
Arlington, VA 22209

Los Alamos Scientific Laboratory
Attn: Report Library
Post Office Box 1663
Los Alamos, NM 87544

Dr. Thomas Weaver
Los Alamos Scientific Laboratory
Los Alamos, NM 87544

Dr. Al Florence
SRI International
333 Ravenswood Avenue
Menlo Park, CA 94025-3493

END

7-87

DTIC